Octopamine and Tyramine Modulate Motor Program Competition in *Drosophila* larvae

William V. Smith[1] and Stefan R. Pulver[1¶]

[1] School of Psychology and Neuroscience, University of St Andrews, St Mary's Quad, South Street, St Andrews KY16 9JP, UK

[¶] Corresponding author: sp96@st-andrews.ac.uk

Abstract

Dynamic Interactions amongst competing motor programs shape behavioural output. Here, we use a combination of opto- and electro-physiology to explore how the *tdc*$^{2+}$ adrenergic-like system modulates competition amongst central pattern generating (CPG) networks controlling locomotion in *Drosophila* larvae. Bath application of octopamine (OA) promoted fictive forwards locomotion, suppressed backwards locomotion, and induced bouts of fictive head sweeps during wash period that were proportional to the promotion of forward waves. In contrast, tyramine (TA), the conceptualised inhibitory antagonist to OA, promoted collisions and overlap of motor programmes, activity-dependent inhibition, and bouts of silence during wash periods. Dual-colour calcium imaging of the *tdc*$^{2+}$ system with motor neurons revealed that the *tdc*$^{2+}$ neurons are recruited phasically prior to a majority of fictive locomotor behaviours. Optogenetic manipulation of the *tdc*$^{2+}$ system recapitulated a subset of effects and further revealed that activity in *tdc*$^{2+}$ system neurons necessary and sufficient for locomotor CPG activity in the system. Overall, our work generates testable predictions for computational and connectomics studies for *Drosophila* motor competition and provides insights into how adrenergic-like systems can modulate dynamics of motor competition among interacting CPGs within locomotor networks.

Introduction

Appropriate locomotion requires both stability and flexibility in neural networks. Locomotion is engendered by not just program initiation but the inhibition of competing motor programs [1]. To balance the need for stability and flexibility, motor systems need to enable appropriate initiation and persistence of locomotion without impairing the capacity to induce alternative motor programs. Given the essential nature of motor adaptability to organismal survival (e.g., escape responses), understanding the general principles of how motor systems manage modulation to motor competition may provide a universal paradigm to examine fundamental network output flexibility. While the role of circuit motifs in specific motor selection and coordination are gradually becoming better understood (e.g. [2]), how neuromodulation underpins competitive selection of motor programs is relatively poorly understood.

The adrenergic-like system in *Drosophila* provides a powerful testbed to evaluate motor competition by enabling controlled, acute modulation to motor bias. The *Drosophila* adrenergic-like system is composed of octopamine (OA) - an invertebrate analogous to adrenaline - and tyramine (TA) [3]. The biosynthetic pathways of OA/TA, their receptor pharmacology [4], [5], and the expression patterns of OA and TA neurons are well studied in multiple invertebrate species [4], [6], [7], [8], [9], [10]. The adrenergic-like system has been implicated in a variety of fundamental behaviours including learning

and memory[11], [12], social behaviours like aggression[13], [14], [15], motor initiation and modulation [9], [16], [17], [18], [19], including fundamental processes underlying action like energy metabolism [20], [21], synaptic plasticity [22], [23], and activity-mediated adaptation [24], [25]. The adrenergic-like system is thus a crucial, multifaceted, and complex system consequential to invertebrate movement and life, especially in its capacity to modulate selection of motor programs.

Traditionally, OA and TA are considered antagonistic neuromodulators [9], [26], [27]. Namely, OA has a well-documented promotive and facilitatory role in locomotion [9], [16], [17], [18], [27], [28], [29], [30], [31], [32] while TA appears to have an overall inhibitory effect on locomotion [6], [8], [27], [33], [34] across invertebrates. However, the functional relationship between OA and TA's action is not always exclusively mutually antagonistic nor definitely excitatory/inhibitory. For instance, the mutual-antagonistic relationship of OA/TA appears to be conditional on their mutual relative concentrations [26]. Further, OA and TA are not always excitatory or inhibitory, respectively. For example, octopamine can have inhibitory effects on CPG activity through inhibition of CPG command interneurons[35], can inhibit nerve-based locomotion stimulation [36], and can inhibit synaptic transmission at the *Drosophila* larval neuromuscular junction [37]. Indeed, different OA receptors are linked to either stimulatory (Octβ2R) or inhibitory (Octβ1R) cAMP/CREB pathways which putatively self-regulates octopaminergic synaptogenesis of boutons at the larval neuromuscular junction [23]. On the other hand, TA can have excitatory effects on neural networks underpinning behaviour. For example, TA can evoke depolarisation through an indirect DA-mediated pathway in rat subthalamic neurons [38], at low concentrations in hyperpolarized states increase the amplitude of locust oviduct excitatory junction potentials stimulating rhythmic contractions [39], and facilitate sensitisation by delaying cocaine-induced responsive hypoactivity [40]. Such research underscores how OA/TA neuromodulation is not exclusively one extreme in a binary view of neuromodulation.

Nonetheless, a significant body of work points to a binary perspective on OA/TA within locomotory systems. One cause of this perspective may be that a majority of prior studies on adrenergic-like modulation have utilised powerful genetic tools (e.g., RNAi, genetic ablation) that often induces long-term changes in the neuromodulatory environments and likely induce undetermined compensation processes during development [41]. Given the highly adaptive, redundant, and complex nature of neural systems, a diverse array of system configurations and features can be somewhat divorced from their ecological contexts [42], [43], [44]. Consequently, chronic genetic manipulations may induce outcomes with complicated interpretations. In contrast, acute modulation of adrenergic-like signalling gives insights into effects that occur moment-to-moment and are not confounded by compensation due to changes in gene expression. Given the high level of characterisation of the adrenergic-like

system in *Drosophila* [45] and the transferability of larval fictive activity to understanding intact locomotion [46], [47], we opted to evaluate the effects of OA/TA on motor competition within CPG networks in *Drosophila* 3rd instar larvae.

A crucial element of movement is action selection and the inhibition of competing motor programs. Appropriate movement is a product of both appropriately sustained driving of CPGs as well as precisely timed and coordinated inhibition of pre-motor networks which drive opposing CPG activity patterns. Indeed, the failure of inhibition between CPG networks may be a direct contributor to uncoordinated and dysrhythmic movement [1]. The role of the adrenergic-like system in modulating action selection and motor pattern competition has been extensively studied in *C. elegans* through tyraminergic RIM neurons [48], [49], [50] which has instantiated a fundamental adrenergic-like motif (i.e., "master-and-slave") in *C. elegans* locomotion. However, while the role of OA/TA has been studied in *Drosophila* with reference to specific program motor initiation and coordination [51], limited work has been conducted on their coordinated role to generalisable motor competition. Through studying the effects of acute modulation on action selection and motor competition, we may be able to gain a more robust, nuanced, and applicable understanding of OA/TA neuromodulatory antagonism.

Here, we explore the role of the tdc^{2+} system modulating fictive motor competition in *Drosophila* larvae to better understand the neural architecture behind CPG coordination. Firstly, we evaluate the intrinsic and modulatory activity of tdc^{2+} system neurons on isolated central pattern generators in 3rd instar *Drosophila* larvae. Specifically, we show that activity in tdc^{2+} neurons and motor neurons is highly correlated during fictive locomotion. Secondly, we demonstrate how bath-applied exogenous OA and TA induce acute changes in CPG acivity during after bath application. Specifically, OA induces elevated fictive forward locomotion in isolated central pattern generators. In contrast, exogenous TA induces increases in motor competition reflective of increased overlapping fictive patterns with activity-dependent inhibitory effects on general fictive activity. Both neuromodulators also induce long lasting effects following bath application that reflect activity changes in the network. Thirdly, through optogenetic manipulation of tdc^{2+} neuronal activity, we demonstrate how intrinsic tdc^{2+} neuronal activity appears sufficient and necessary for producing fictive rhythms. Finally we show how regionally restricted depolarisation of tdc^{2+} neuronal activity in the posterior abdominal isolated ganglion is sufficient to induce fictive forward activity. Overall, we demonstrate how the adrenergic-like system is a valuable tool for understanding the secondary effects of modulating motor competition

121 # Methods

122 ## Animal Rearing & Dissection

123 *Drosophila* were raised at 18-25∘C in incubators on an approximate 12-hour light-dark cycle. All
124 experiments were conducted with feeding 3rd instar *Drosophila* larva (2-3 days posthatching). The
125 central nervous system (CNS) of *Drosophila* was isolated as reported in [46]. Activity of isolated CNSs
126 was recorded with Baines External Saline (BES) submersion containing (in mM) 135 NaCl, 5 KCl, 2 $CaCl_2$,
127 4 $MgCl_2$, 5 TES, and 36 sucrose, pH 7.15 [52]. All CNS preparations were isolated from *Drosophila* larva
128 using dorsal incision across the larva body using fine scissors with body walls pinned into a Sylgard-
129 lined Petri dishes using fine tungsten wires (California Fine Wire, Grover Beach, CA). All projecting CNS
130 nerves were cut, CNS removed, posterior nerves and peripheral gastric tissue attached were pinned
131 using fine tungsten wires (see [46]).

132 ## Dual Colour Ca^{2+} Imaging of *Tdc*$^{2+}$ and Motor Neurons

133 The calcium activity patterns of motor neurons and *tdc*$^{2+}$ neurons [53] were assessed in isolated CNS
134 feeding 3rd instar *Drosophila* larva using a genetic construct that drove RCaMP1a expression in
135 glutamatergic neurons (VGlut-LexA combined with 13XLexAOP-RCaMP1a balanced over CyO, Tb-RFP),
136 while also containing UAS-GCaMP6f (provided by K.L. Hibbard, janelia Reserch Campus) This construct
137 was then crossed to w[*]; P{w[+mC]=Tdc2-GAL4.) Isolated CNS *Drosophila* were imaged using an
138 OptoSplit Imaging system (Cairn Research Ltd, Kent, UK) with appropriate excitation and emission
139 filters for RCAMP and GCAMP imaging. Preparations were imaged using an OLA light engine
140 (Lumencor, OR, USA) and an ORCA-Fusion CMOS camera (Hamamatsu, Hamamatsu, Japan) with a
141 XLUMPLFLN 20X dipping objective (Olympus, Tokyo, Japan). We imaged isolated dual-colour CNS
142 *Drosophila* with BES using an X-light spinning disk confocal with a 70µm pinhole array (Crest Optics,
143 Rome, Italy) for up to 30 minutes at 5fps with 150ms exposure. Images were collected using
144 MicroManager (v2.0 gamma [54]) and post-processed using ImageJ [55], [56]. The channels displaying
145 the calcium activity for motor neurons and *tdc*$^{2+}$ neurons were overlayed using each segment's nerve
146 roots as a reference marker. All calcium signals were extracted using area-consistent regions of
147 interest on nerve roots projecting from ventral nerve cord segments (T3-A6) (Figure 1Aii). All calcium
148 signals were pre-processed (df/f) and smoothed using a custom Python script (see data repositor for
149 details) Fictive events were determined through using Hill's Valley Analysis in DataView [1] and/or
150 SciPy's peak detection algorithm based on criteria reported in [46].

151 Visualisation of dual-colour calcium data was performed in DataView and Python3 using scripts
152 available in paper-associated repositories. The overlaid average calcium activity trace in *tdc*$^{2+}$ and

153 motor neurons (as shown in Figure 1C) was performed using DataView's event-scope view based on
154 segregated fictive events detected by Hill's Valley analysis across all preparations based on criteria
155 reported in [46]. The average waveform of each event was calculated by DataView and extracted into
156 Python for across preparation visualisation. All average waveforms were determined using a duration
157 threshold of 8300ms. The peak time lag calculation (as shown in Figure 1D) was the difference in peaks
158 from the average waveform of *tdc*$^{2+}$ and motor neurons in each segment using SciPy's peak detection
159 algorithm (see repository code). Fictive events in calcium traces were determined using Hill's Valley
160 analysis and manually counted as reported in [46]. Peak and duration relation between *tdc*$^{2+}$ and
161 motor neuron calcium signals (as shown in Figure 1G) was performed using Hill's Valley detection on
162 each segment across all preparations with duration calculated as 20% on-off from the centre of the
163 calcium signal. The correlation between *tdc*$^{2+}$ and motor neuron calcium signals (as shown in Figure
164 1E) was conducted using Pearson Cross Correlation coefficient across all preparations through
165 Python's Scipy.Signal package (see repository code).

166 **Ca^{2+} Imaging with Tyramine & Octopamine Perfusion**

167 The effect of exogenous octopamine bath application on calcium signals in motor neurons was
168 assessed in isolated CNS feeding 3rd instar *Drosophila* larvae using a genetic line in which GCaMP6m is
169 driven in glutamatergic neurons by the OK371-GAL4 line. Isolated CNS preparations were pinned to
170 Sylgard-lined Petri dishes as described in "Dual Colour Ca^{2+} Imaging of *tdc*$^{2+}$ and Motor Neurons".
171 Saline and OA or TA were applied during imaging using a gravity-based perfusion system with a
172 consistent drip inflow across preparations and removed continuously using a KCP3-B10W peristaltic
173 pump (Kamoer 60-120 RPM). Across all preparations, saline was bath applied onto the preparation for
174 at least 10 minutes followed by 10-minute OA or TA application then < 20 minutes saline reapplication
175 to wash away octopamine/tyramine from the Sylgard-lined Petri dish. All OA concentration ranges (5
176 - 400µM) were generated from a diluted 0.02M master mix (O0250-1G Sigma Aldrich). All
177 TAconcentration ranges (5 - 400µM) were generated from a diluted 0.01M master mix (T90344-5G
178 Sigma Aldrich). Images were collected using WinFluor (University of Strathclyde, UK) at 10fps and post-
179 processing using ImageJ [55], [56]. All isolated preparations were recorded using a UPlanFLN Olympus
180 10x, 0.3nA.

181 ***Tdc*$^{2+}$ Optogenetics**

182 The effect of endogenous *tdc*$^{2+}$ activity on fictive motor activity was studied using extracellular
183 electrophysiology on segmental nerve roots in isolated CNS from feeding 3rd instar *Drosophila* larvae.
184 Octopaminergic *tdc*$^{2+}$ neurons were either depolarised using lines containing 20xUAS-CsChrimson-
185 mVenus inserted at the attP18 landing site or hyperpolarized using lines containing UAS-GtACR1

186 inserted in VK00005 driven by w[*]; P{w[+mC]=Tdc2-GAL4. Across all conditions, the activity of
187 thoracic nerve root (T3) and posterior abdominal nerve root (A6-A8) was measured by suction
188 electrode recording (AM System Differential AC Amplifier Model (#59721, 1700), 1-100kHz cut-off
189 frequency allowance). Borosilicate glass capillaries were pulled using an electrode puller (Narishege,
190 Japan), and tapered tips were broken to produce suction electrodes that fit tightly around single nerve
191 roots. Stimulation during the *tdc*$^{2+}$-CsChrimson conditions was performed with a downward-projecting
192 red LED light source (Cairn Research Ltd., 620 nm, 0.58mW/cm^2). The stimulation period was either
193 consistent for 10, 20, or 40s or discontinuous with 0.01s pulses generated at intervals of 40Hz for ~10s
194 total pulsed stimulation. Stimulation during the *tdc*$^{2+}$-GtACR1 conditions was performed with upward-
195 projecting white light (~2.5mW/cm^2). The stimulation period was consistent for ∽15, 30, or 60s
196 induced by manual instantiation. All whole-prep stimulation used full-prep illumination using a
197 UPlanFLN Olympus 10x, 0.3nA lens.

198 Restricted illumination stimulation conditions involved restricting the downward-projecting red light
199 source using a light-path restrictor with ∾0.6cm aperture and 0.16mW/cm^2 power-to-area ratio.
200 Restricted stimulation involved a LUMPlanF Olympus 40x, (0.8 nA) dipping lens focused on posterior
201 abdominal, anterior abdominal, thoracic, and suboesophageal ganglion regions (see Figure 6). Aside
202 from direct restricted prep stimulation, all conditions were matched with control stimulation where
203 illumination of the left-flank of the preparation (< 1cm) was conducted during nerve root recording.

204 All electrophysiology recordings and light stimulations were made using LabChart 8.0 software (AD
205 Instruments, Colorado Springs, CO) and post-processed in Spike2 (Cambridge Electronic Design,
206 Cambridge, UK) and Python3. Post-processing involved rectification and smoothing using a consistent
207 0.2s time interval. All rectified and smoothed traces were imported into DataView where event peaks
208 and 20% on-off duration were determined by Hill's Valley analysis. Visualisation and further analysis
209 were conducted in Python3 (see repository code).

210 Analysis, Visualisation, & Statistical Evaluation

211 All calcium signal and electrophysiology nerve root data were initially analysed in DataView (version
212 12.2.2)[57] using Hill's Valley Analysis for peak detection and Event-Triggered Scope View for
213 averaging waveforms. All data were visualised in Python3 using custom scripts available in the
214 repository supplied by the authors. All statistical tests were performed using packages within Python
215 (see repository scripts and report tests in the results sections).

Results

Tdc^{2+} VNC Neuron Activity is Correlated to Motor Neuron Activity across all Fictive Motor Programs

The isolated *Drosophila* central nervous system (CNS) spontaneously generates fictive motor rhythms in the thoracic and abdominal segments that can be measured via calcium indicators expressed in neuronal populations[46]. Previous work has characterised the features and relationship between fictive activity patterns using different genetically-encoded calcium indicators [1], [46], [47], [58]. Succinctly, isolated CNS preparations display fictive forwards and backwards motor programmes characterised by anterior-to-posterior or posterior-to-anterior progression of activity in motor neuron segments, respectively. In addition, preparations also can display fictive bilaterally symmetric activity in the anterior thoracic and posterior abdominal segments indicative of head raising or tail grounding behaviours, respectively. Finally, preparations can display bilaterally asymmetric activity in the anterior thoracic indicative of headsweep-like behaviours in intact *Drosophila* larva. OA is manufactured and released from neuronal subpopulations in the suboesophageal ganglion and ventral nerve cord expressing the *tdc2+* gene [9] with staining suggesting the brain contains only TA, and no OA-immunoreactive cells [59]. Given both chronic and acute manipulations can have a profound effect on locomotion, we first evaluated if activity of OA neurons in the ventral nerve cord (VNC) - indicative of TA and OA release - was correlated with fictive motor rhythms. There exist subpopulations of distinct octopaminergic neurons that line the ventromedial (T3-A6) axis of the CNS[9]. Through expressing different calcium indicators in VNC motor neurons (VGlut, RCaMP1a) and ventromedial *tdc*$^{2+}$ neurons (TDC^{2+}, GCaMP6f) (Figure 1Aii), we explored the intrinsic relationship between VNC *tdc*$^{2+}$ neurons and motor neurons during spontaneous fictive activity bouts. The calcium activity of motor neurons and *tdc*$^{2+}$ neurons in each VNC segment showed high correlation across different fictive motor programs (Figure 1B).

By parsing all instances of fictive events across dual-colour preparations (N=7), we can see a robust similarity in *tdc*$^{2+}$ and motor neuron temporal activity within each segment (Figure 1C). Specifically, if we take the average calcium activity trace for all segments for motor neurons and *tdc*$^{2+}$ neurons for all fictive activity patterns, we see they have consistent similarity and phase locking for all fictive motor categories. The strong association between activity in motor neurons and *tdc*$^{2+}$ neurons is more apparent when comparing activity peaks between each neuronal population in each segment per each unique fictive behaviour (Figure 1D). The temporal relationship between motor neuronal and *tdc*$^{2+}$ neurons showed variations depending on the fictive motor program. At the initiating segment for fictive activity, mean$\pm$SEM motor neuron activity on average preceded *tdc*$^{2+}$ neuron activity for

249 forward (462±704 ms at A6, N=5), posterior burst (449±614 ms at A6, N=5), and anterior burst
250 (235±352 ms at T3, N=2) fictive events. In contrast, *tdc*$^{2+}$ neuron activity preceded motor neuron
251 activity in initiating segments for fictive backward (432±786 ms at T3, N=3), right asymmetric (9±38
252 ms at T3, N=2), and left asymmetric (99±57ms at T3, N=3) events. Importantly, any initiating segment
253 peak difference relationship between motor neurons and *tdc*$^{2+}$ neurons is not consistent across
254 segments for fictive forward and backward activity events. For example, as fictive forward motor
255 activity progresses to the anterior regions (A2 - T3) of the CNS, average *tdc*$^{2+}$ neuron peak activity now
256 precedes motor neuron activity (Figure 1B, D). In short, while there is some inter-prep variability
257 between the temporal organisation of motor neuron and *tdc*$^{2+}$ neuron peak activity, there is a strong
258 coupling between the activity of these two neuron subpopulations in all fictive behaviours; in all fictive
259 patterns, there is a complete ipsilateral mirror-image of activity across all segments even if the lag
260 relationships show intersegmental differences.

261 *Tdc*$^{2+}$ neurons show fictive-like activity patterns both commensurate with but also independent of
262 motor neuron activity. The majority of fictive motor events across preparations showed
263 commensurate *tdc*$^{2+}$ neuron activity events. Across all preparations, 69% of fictive forward waves and
264 anterior asymmetric events, 76% of posterior burst events, and 100% fictive backward waves showed
265 commensurate *tdc*$^{2+}$ activity in a close time window (< 5s) and same segment-to-segment relationship
266 that classically defines the fictive motor programs (Figure 1E). Noteably, there was a large variability
267 in recruitment between preparations that underestimates the overall level of recruitment displayed
268 by some preparations. For instance, in 4 out of 6 preparations there was >90% fictive forward
269 recruitment. In short, most fictive motor patterns have commensurate *tdc*$^{2+}$ neuron patterns but there
270 are excess motor patterns not matched in *tdc*$^{2+}$ patterns. Similarly, there are excess fictive-like *tdc*$^{2+}$
271 activity patterns that occur without commensurate fictive motor patterns in the network (Figure 1F).
272 Across preparations, there are excess *tdc*$^{2+}$ activity patterns reminiscent of all types of fictive-like
273 activity events. For instance, across all preparations there were 7.8% more backwards-like activity
274 patterns in octopaminergic neurons than backward fictive motor activity patterns despite 100%
275 recruitment per preparation. Similarly, per preparation, there were 8.7%, 5.4%, 1.8%, 2.1% excess
276 *tdc*$^{2+}$ recruitment for anterior burst, anterior asymmetric, fictive forward, and posterior burst activity,
277 respectively.

278 Independent of fictive events, the activity in motor neurons and *tdc*$^{2+}$ neuron pools per segment are
279 highly correlated. Specifically, the quantity of motor neuron and *tdc*$^{2+}$ neuron calcium activity peaks
280 (r_s = 0.82, p < .001) (Figure 1Gi) and duration (r_s = 0.81, p < .001) (Figure 1Gii) of activity within each
281 segment were highly correlated. Pearson correlation between motor neuron and *tdc*$^{2+}$ neuron calcium

activity per segment demonstrated an average, moderately positive correlation (r = 0.4) but with considerable intersegmental and lateral variability (Fisher's Z Score = 0.44 with 0.27 variance). Overall, activity of motor neurons and *tdc*$^{2+}$ neurons are highly correlated. When fictive motor events occur, there is likely a commensurate, almost synchronous *tdc*$^{2+}$ signal as the event propagates in the VNC but there are occasions when both fictive motor events and *tdc*$^{2+}$ fictive-like events appear to occur independently.

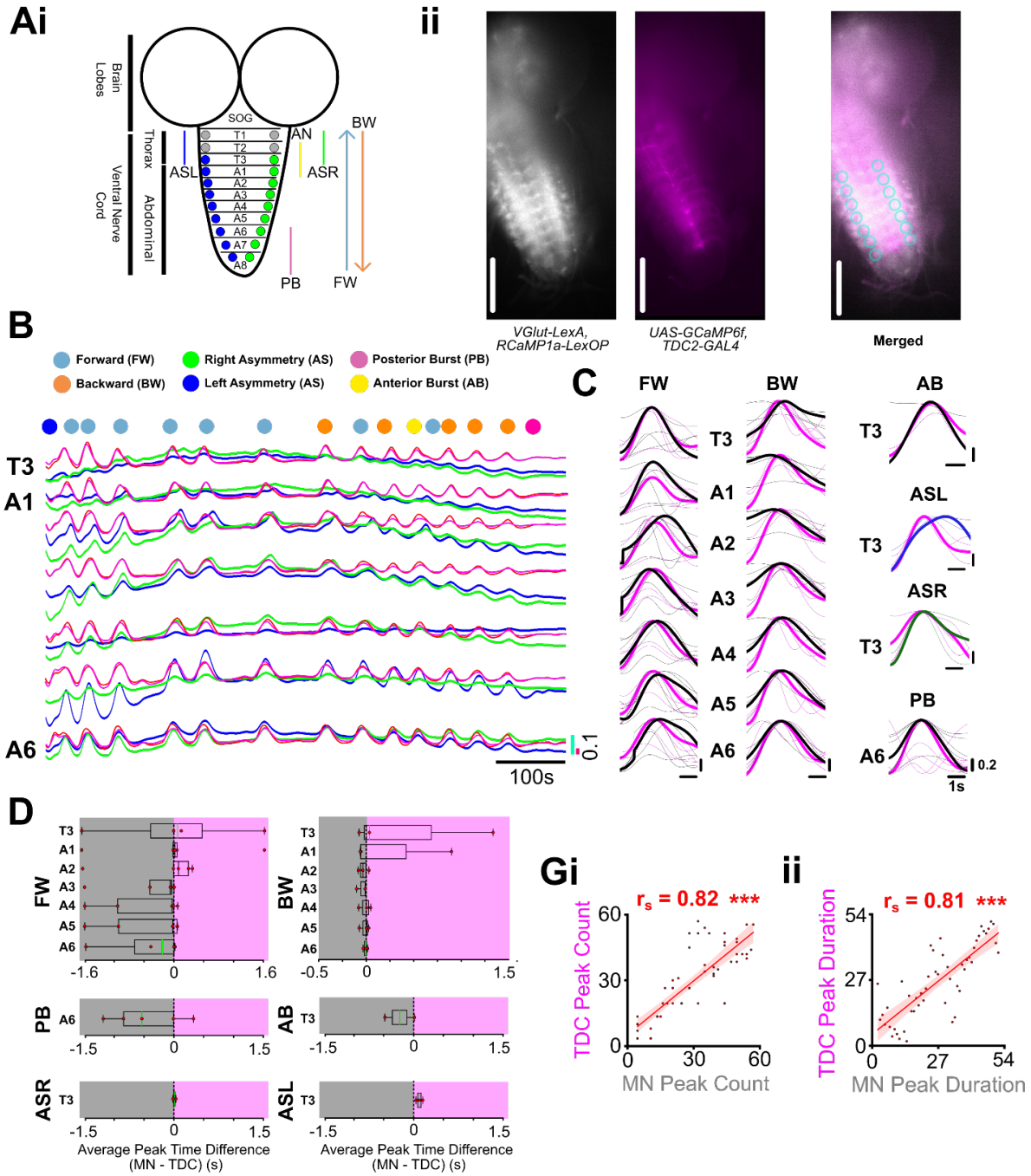
Ai
Brain Lobes
Ventral Nerve Cord
Thorax
Abdominal
SOG
T1
T2
T3
A1
A2
A3
A4
A5
A6
A7
A8
AN
ASL
ASR
BW
PB
FW
ii
VGlut-LexA, RCaMP1a-LexOP
UAS-GCaMP6f, TDC2-GAL4
Merged
B
Forward (FW)
Backward (BW)
Right Asymmetry (AS)
Left Asymmetry (AS)
Posterior Burst (PB)
Anterior Burst (AB)
T3
A1
A6
100s
0.1
C
FW
BW
AB
ASL
ASR
PB
0.2
1s
D
Average Peak Time Difference (MN - TDC) (s)
Gi
ii
r_s = 0.82 ***
r_s = 0.81 ***
TDC Peak Count
MN Peak Count
TDC Peak Duration
MN Peak Duration
E
Recruitment (%)
Fictive Behaviour
F
MN
TDC
Behaviour
Event Count
H
L
R
Segment
Correlation

288

Figure 1: High Activity Correlation between *tdc*$^{2+}$ VNC and Motor Neurons in the Same Segment and Fictive Pattern

(**Ai**) The isolated ventral nerve cord (VNC) demonstrates sequences of motor neuron activity resembling activity patterns underlying locomotion in intact animals (i.e., "FW" = fictive forward, "BW" = fictive backward, "AN" = anterior burst, "PB" = posterior burst, "ASR" = asymmetric right, "ASL" = asymmetry left). (**Aii**) Intrinsic calcium activity of motor neurons (MN) and octopaminergic neurons (TDC) is evaluated through dual calcium indicator expression at nerve root regions of interest (blue circles) T3 - A6. Dots above the traces indicate the initiation of the different fictive behaviours (light blue, fictive forward; orange, fictive backward; yellow, anterior symmetric burst; pink, posterior burst; blue, left anterior asymmetry; green, right anterior asymmetry). Lines indicate baseline-correct calcium fluorescence values (green/blue = right/left MN in each segment, magenta/red = right/left *tdc*$^{2+}$ VUM in each segment) (**B**) Exemplar calcium trace of MN (left = blue, green = right) and *tdc*$^{2+}$ neurons (left = magenta, right = red) demonstrating strong association between MNs and Tdc2+ neuron activity within each ventral nerve cord (VNC) segment. (**C**) Averaged calcium image traces of *VGlut RCaMP1a* (black), *Tdc2*$^{+}$ *GCaMP6f* (magenta) for fictive forward (FW), backward (BW), anterior burst (AB), left asymmetry (blue, ASL), right asymmetry (green, ASR), and posterior burst (PB) activity. Bold traces represent average across all preparations (N = 7) with each individual prep average calcium trace in non-bold. The calcium signal amplitudes are normalised within each fictive behavioural class. (**D**) The time difference between the peaks in the MN and TDC calcium trace within each preparation, across fictive patterns and ventral nerve cord segment (T3 - A6). Negative average peak time differences occur when the average prep MN trace proceeds the TDC signal in the segment, positive average peak time represents TDC proceeding MN signals in the segment. Green line represents the average peak time difference across all preparations in the most distal VNC segments. (**E**) The % event count where a motor neuron fictive pattern exists alongside a corresponding TDC activity pattern across different fictive activity categories (with standard error bars). (**F**) The count of fictive activity patterns demonstrated by MN and TDC VNC populations. Note in many fictive activity patterns there is an excess of TDC exhibitions compared to motor fictive patterns. (**G**) An agnostic measure of MN and TDC signals pooled across segments and preparations showing the Spearman's Rank for (**i**) peak count comparison and (**ii**) 20% on-off peak duration comparison. (**H**) Pearson correlation coefficient for the MN and TDC traces of each segment within all preparations for the left (blue) and right (green) axis of the VNC. Comparisons followed by post-hoc was conducted with p-values: < .5 (*), < .01 (**), <.001 (***) shown. Only statistically significant bars are shown.

Bath Application of OA induces Fictive Forward & Long-lasting Anterior Asymmetric Activity

Given the high correlation between intrinsic *tdc*$^{2+}$ neuron CNS and spontaneous motor activity, we next turned to evaluate the effects of OA on fictive motor bouts. Exogenous application of OA to intact invertebrates has a well-reported role as a promoter of locomotion aligned with fight-or-flight responses across species [4], [11]. Here, we explored how exogenous application of OA shapes locomotory networks devoid of sensory feedback to better understand the role of OA on coupled oscillatory circuits and motor competition.

The exogenous application of OA altered the fictive landscape of the isolated VNC preparation from fictive variability to nearly exclusive fictive forward motor patterns (Figure 2A). Application of OA concentrations ≥100μM significantly promoted fictive forward activity (100μM 5.4$\pm$2.0m^{-1} p = .003;

329 200µM 6.5±3.2m^{-1} p < .001; 400µM 14.9±6.4m^{-1} p = .004) compared to saline pre-application (100µM
330 0.7±0.4m^{-1}; 200µM 0.7±0.7m^{-1}; 400µM 0.8±0.7m^{-1}) (Figure 2Ci). At OA concentrations ≥200µM, the
331 induction of fictive forward bias came at the expense of fictive backward motor activity which was
332 significantly reduced (200µM 0.2±0.6m^{-1} p = .005; 400µM 0.6±0.7m^{-1} p = .004) compared to saline
333 pre-application (200µM 1.4±0.5m^{-1}; 400µM 2.3±0.9m^{-1}) (Figure 2Cii). Interestingly, anterior
334 asymmetric events were significantly promoted at higher OA concentrations >400µM (Figure 2Cv).
335 However, the significant elevation in anterior asymmetric activity was not induced during the 10-
336 minute OA application but only after the OA wash and thus consequent to the neuromodulator
337 induced fictive forward bias (Figure 2A, Cv). Importantly, while OA did not appear to significantly
338 potentiate anterior asymmetric fictive activity in a concentration-dependent manner, there was a
339 trend to increased anterior asymmetric activity with increasing OA concentration. Interestingly, OA
340 induced long-lasting elevated anterior asymmetric activity whose activity trend peaks 35.7±16.9
341 minutes post the start of the OA wash. Noteworthily, as anterior asymmetric activity is not promoted
342 at lower OA concentrations, we can be confident that the post-application effects are not an artefact
343 of diminishing OA during the gradual wash period. Taken together, we can conceptualise OA
344 neuromodulation as restraining motor competition via biasing the network to fictive forward
345 locomotion. By exploring fictive transitions (i.e., the probability of making a transition from one motor
346 program to another), we can see that OA's forward bias is reflective of a significant decrease in fictive
347 transitions programs that would transition the network away from, and thus reinforce programs
348 towards, fictive forward motor patterns (Supplementary Figure 1B). Overall, exogenous application of
349 OA appears to collapse fictive activity diversity, tuning the network into fictive forward bias mode with
350 consequent post-application motor bias to non-wave-like activity.

351 To understand the relationship between OA's induction of fictive forward bias and the post-
352 application anterior asymmetric fictive activity, we examined the relative changes in fictive frequency
353 between different motor programs across all concentrations (Figure 2E). Intriguingly, the more
354 exogenous OA promoted fictive forward bias, the greater the post-application anterior asymmetric
355 activity relative to pre-application (Figure 2Ei, r_s = 0.5, p < .001). This proportional relationship was not
356 exhibited between any other fictive event. Interestingly, the proportional increase in anterior
357 asymmetric activity with respect to fictive forward bias appears significantly conditional on the relative
358 promotion of anterior asymmetric activity during OA application (Figure 2Eii, r_s = -0.4, p = .002). Put
359 simply, the greater fictive forward bias promoted by OA, the more fictive anterior asymmetric activity
360 is delayed until the network is no longer forward biased (Figure 2Evi ,R^2 = 0.4 p < .001). In effect, it
361 appears that post-OA promotion of anterior asymmetric events is a product of OA evoking greater
362 fictive forward bias in the isolated preparation at the expense of anterior asymmetric events. During

363 OA application, the induced fictive forward bias is regularly interspersed with a few anterior
364 asymmetric events (Figure 2A, Octopamine, "FW // AS Transitions"). Taken all together, this implies
365 that fictive forward bias immediately potentiates anterior asymmetric activity, but the former
366 dominates the fictive landscape over the latter until OA's removal removes the neuromodulatory
367 potentiation of fictive forward activity.

368 Aside from changes in the frequency of fictive events at the CPG level, OA induces significant decrease
369 in the amplitude of the calcium signal without a noticeable change in signal baseline as previously
370 reported by [60] (Figure 2Aii, Supplementary Figure 1A-E). The reduction in calcium amplitude was
371 reflected by a reduced duration in motor root bursting during OA application in both thoracic and
372 abdominal motor pools demonstrating the amplitude change in the calcium signal is reflective of OA-
373 induced shorter motor neuron bursting (Supplementary Figure 1F-H).

374 We next evaluated how the OA-induced faster rhythms exhibited in intact *Drosophila*[27] are
375 represented in the isolated motor circuit. Exogenous bath application of OA qualitatively decreased
376 intersegmental propagation delay for fictive forward and turn but not fictive backward activity (Figure
377 2D). Fictive forward wave (Figure 3Di) and turn wave (Figure 3Diii) duration is significantly shorter with
378 exogenous OA application. Specifically, all OA concentrations ≥50µM significantly increased forward
379 wave speed (50µM 4.4±2.4s $p = .05$; 100µM 3.6±1.3s $p < .001$; 200µM 3.7±1.4s $p = .002$; 400µM
380 1.7±0.7s $p = .01$) compared to pre-application saline perfusion (8.4±8.3s). Similarly, octopamine
381 concentrations ≥200µM significantly increased turn wave speed (200µM 3.2±1.6s $p = .01$; 400µM
382 1.6±1.4s $p = .03$) compared to pre-application saline perfusion (7.0±1.9s). OA did not induce any
383 significant changes in fictive backward wave speed. Thus, OA biases the isolated *Drosophila* CNS to
384 fictive forward locomotion consequently restricting motor diversity, induces faster CPG bursting, and
385 potentiates intersegmental propagation between segments that affects some system-wide activity
386 progression. More subtly, given that lower OA concentrations could significantly affect selective
387 intersegmental propagation but not overall fictive frequency, these data imply OA can modulate
388 locomotory speed independent of modulating initiation bias.

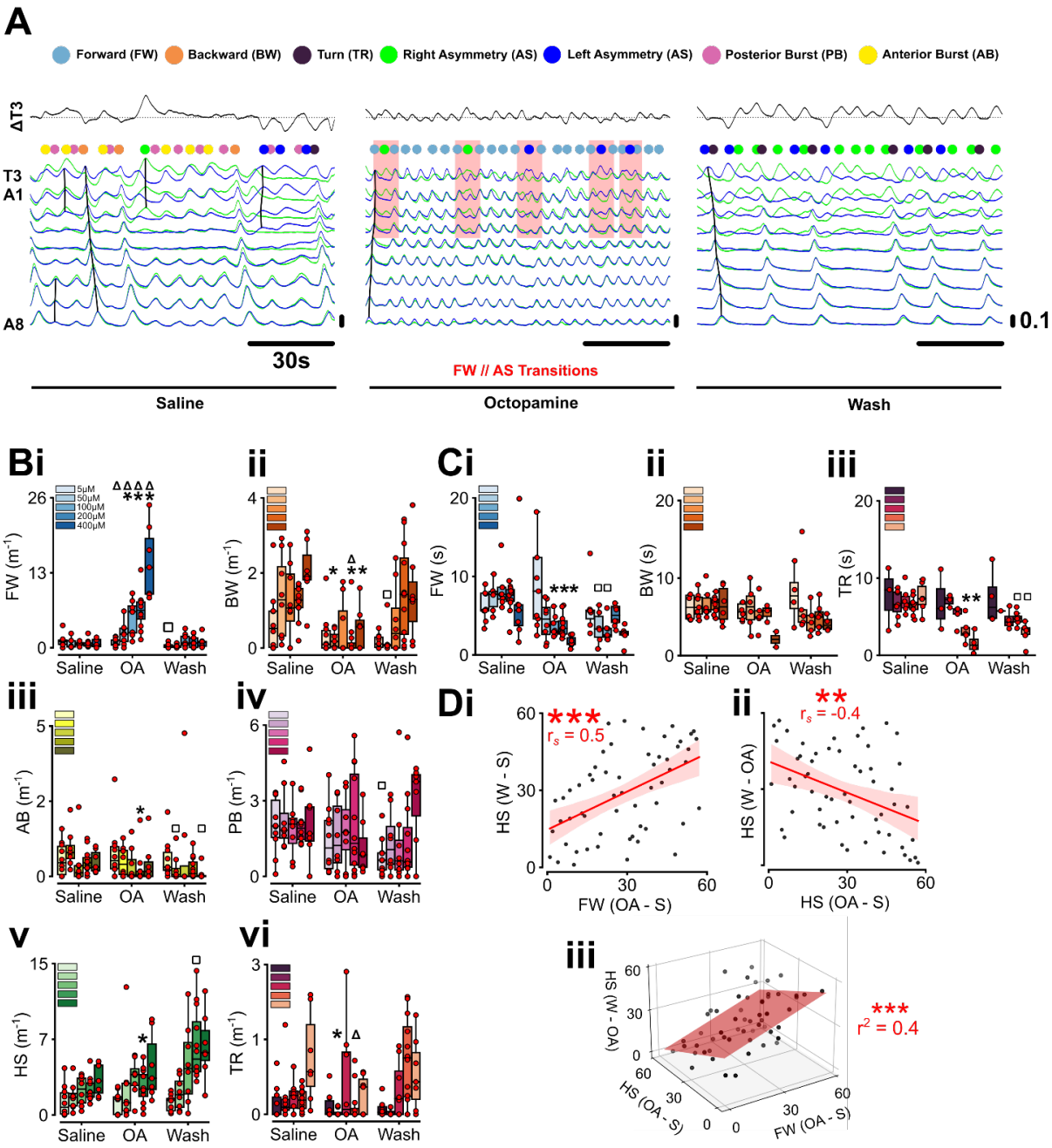

Figure 2: Bath Application of OA Induces Fictive Forward Bias in the isolated larval CNS

(**A**) Exemplar calcium dynamics in left (blue) and right (green) motor neurons in the 3rd instar isolated *Drosophila* ventral nerve cord (VNC) over 45 minutes under saline, octopamine (OA) (200μM), wash bath applications. Difference trace for T3 (ΔT3) shown above all traces (left - right). Dots above the traces indicate the initiation of the different fictive behaviours (light blue, fictive forward; orange, fictive backward; yellow, anterior symmetric burst; pink, posterior burst; blue, left anterior asymmetry; green, right anterior asymmetry). Black lines indicate the shape of each fictive activity to aid user's recognition of fictive programmes. Note that octopamine application induces fictive forward bias with intermittent asymmetric activity with the post-application wash period exhibiting dominating anterior asymmetric activity. (**B**) Changes in fictive frequencies of different fictive behaviours under the application of OA concentrations (5 - 400μM) between saline, OA perfusion, and wash conditions for fictive: (**i**) forward , (**ii**) backward, (**iii**) anterior burst, (**iv**) posterior burst, (**v**) anterior asymmetric headsweeps, and (**vi**) turn. Note that the axis showing the rate of each fictive activity is different for each fictive activity. (**C**) Activity propagation speed from

402 posterior (A8) to anterior (T3) for (**i**) fictive forward and anterior-to-posterior for (**ii**) fictive backward and (**iii**) fictive
403 turning behaviours. (**Ei**) Ranked relationship between the relative effect of OA on promoting fictive forward activity
404 and the relative change in headsweep asymmetric. (**Eii**) Ranked relationship between the relative promotion of
405 anterior asymmetric activity by OA and the change in anterior asymmetric activity in wash relative to OA application
406 activity level. (**F**) Ranked relationship between relative promotion of fictive forward waves by octopamine during
407 application (X variable, FW (OA-S)), relative promotion of anterior asymmetric activity during octopamine
408 application compared to the activity in the pre-application time window (Y variable, HS (OA-S)), and relative change
409 in anterior asymmetric activity between the octopamine application and post-application time window (Z variable,
410 HS (W-OA)). Z = 0.45*X + -0.44*Y + 27.78. Note the fact that fictive forward promotion in octopamine comes at the
411 expense of asymmetric anterior headsweep activity. Significant post-hoc comparisons are exclusively shown
412 denoted by ☐ saline vs wash, ✳ saline vs OA, Δ OA vs wash.

413 **Tyramine Bath Application Induces Fictive Overlap & Motor Competition**

414 *Tdc*$^{2+}$-expressing neurons are capable of synthesising and releasing both OA and TA [7], [8], [10], [59].
415 Given the highly active coupling of intrinsic *tdc*$^{2+}$ activity and motor activity and OA's excitatory effect
416 on fictive activity, we next evaluated the role of TA on CPG activity and motor competition. TA is
417 considered antagonistic to OA modulation with evidence of TA's inhibitory role on intact locomotion
418 [27] and motor electrophysiology [34]. Thus, we turned to explore whether TA has a universal
419 inhibitory role on motor competition in isolated preparations to better understand how behavioural
420 inhibition manifests at a CPG and network level via *tdc*$^{2+}$ activity.

421 We explored the effect of TA on motor competition by exogenously bath applying TA onto isolated 3rd
422 instar larva VNC as in our OA experiments. Unlike OA, TA did not induce a consistent motor bias across
423 applied concentrations compared to pre-application (Figure 3A, B). Across all fictive behavioural
424 patterns, the only significant fictive changes occurred post-TA application. Specifically, fictive forward
425 (200µM 0.6$\pm$0.4m^{-1} $p < .001$) and posterior burst (400µM 0.7$\pm$0.6m^{-1} $p < .001$) activity was
426 significantly reduced in the wash period relative to the TA application period (FW, 200µM 10.3$\pm$8.1m^{-}
427 ^{1}) or pre-application saline period (PB, 200µM 18.7$\pm$11.5m^{-1}) respectively. Further, again in contrast
428 to OA, TA did not induce any significant changes to the intersegmental propagation of neither fictive
429 forward, backward, nor turn behaviours (Figure 3C). Reflective of this insignificant change in fictive
430 incidences, TA perfusion appears to not induce significant, widespread changes in the landscape of
431 fictive transitions (Supplementary Figure 2B). In fact, in some instances, TA perfusion significantly
432 increased motor transitions reflective of subtle increases in motor competition and thus overall fictive
433 program diversity.

434 While TA did not induce fictive bias in the isolated network, TA perfusion induced a significant increase
435 in the overlap of fictive motor programs (Figure 3A, Tyramine "Overlap") represented by increased
436 overlap in activity across at least one ventral nerve cord ganglion segment (Figure 3D). Perfusion of

200µM TA induced a significant increase in time the network demonstrates activity overlap across at least one segment (6.2±0.4% p = < .001) compared to the 0% overlap demonstrated during the pre-tyramine application period. Aside from overlap promotion, the application of ≥100µM TA induced a significant decrease in the activity in the post-application in a concentration-dependent manner (100µM 84.5±4.8% p = .01; 200µM 49.8±31.7% p = .002; 400µM 56.4±12.3% p = .006) compared to pre-application period (100µM 95.4±3.8%; 200µM 93.2±9.8%; 400µM 97.7±2.2%) (Figure 3A, Wash "Silence"; Figure 3Ei). Similar to our prior analysis evaluating correlations between fictive changes by the OA and the post-application anterior asymmetric increase, we turned to correlation analysis between activity and silence to attempt to understand the long-lasting modulatory effects of TA. However, we did not find any significant relationship between activity changes by TA perfusion and the relative changes in activity in the post-application wash period (Figure 3Eii). Further, there was no significant relationship between the overlap and the post-application silence promoted by TA (Figure 3Eiii). Given prior work has drawn attention to the state-dependent effects of TA inhibition[26], we next evaluated if TA's effects on fictive activity were dependent upon the activity state prior to TA application. As shown in Figure Eiv, TA did exhibit proportional and increasing inhibitory effects as overall fictive activity levels rose beyond pre-application activity levels > $6.7m^{-1}$ ($p = .04$, $r^2 = 0.2$). Further more, when baseline activity is low, TA can actually have excitatory effects. Taken together, TA promotes overlaps between different fictive motor programs and demonstrates activity-dependent inhibition of overall fictive activity and

Given that previous work has indicated an inhibitory role for TA at an individual cellular level[26], [48] we evaluated the effect of TA perfusion on motor nerve root bursting activity. Unexpectedly, TA perfusion induced a trend, albeit marginally insignificant, towards an increase in motor root bursting (Supplementary Figure 3Ai, ii) with no significant effects on bursting duration (Supplementary Figure 3Aiii), overall duration of inactivity (Supplementary Figure 3Aiv), bursting amplitude (Supplementary Figure 3Av), or tonic baseline amplitude (Supplementary Figure 3Avi). 200µM TA application induced a significant reduction (p = .001) in the amplitude of calcium activity (Figure 3A, Supplementary Figure 3Bi, iii) without, similar to OA, any changes to the baseline calcium activity (Supplementary Figure 3Bii, iv).

Overall, TA application to the isolated network is inhibitory on rhythm generation at higher activity states but excitatory at lower activity states. I Further, TA appears to facilitate the overlapping of fictive motor programs with prolonged reduction in overall activity absent inhibition at the motor neuron population level.

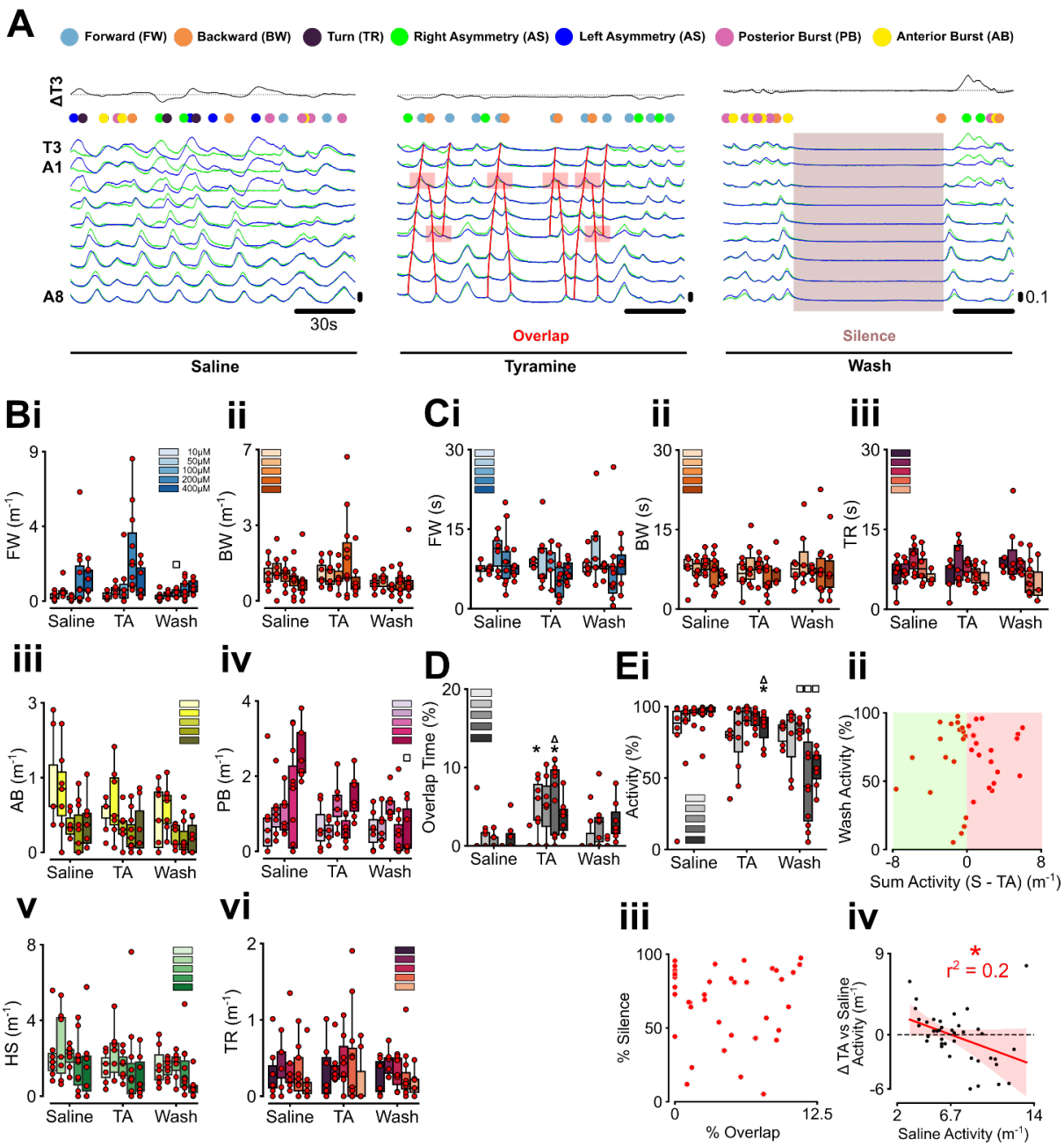

Figure 3: Bath Application of TA Induces Fictive Motor Overlap and Competition

(**A**) Exemplar calcium dynamics in left (blue) and right (green) motor neurons in the 3rd instar isolated *Drosophila* ventral nerve cord (VNC) over 45 minutes under saline, tyramine (TA) (200μM), wash bath applications. Note the overlap between fictive forward and backward motor activity (red) during tyramine application and absence of fictive activity in the wash period. (**B**) Changes in fictive frequencies of different fictive behaviours under the application of TA concentrations (10 - 400μM) between saline, TA perfusion, and wash conditions for fictive: (**i**) forward , (**ii**) backward, (**iii**) anterior burst, (**iv**) posterior burst, (**v**) anterior asymmetric headsweeps, and (**vi**) turn. Note that the axis showing the rate of each fictive activity is different for each fictive activity. (**C**) Activity propagation speed from posterior (A8) to anterior (T3) for (**i**) fictive forward and anterior-to-posterior for (**ii**) fictive backward and (**iii**) fictive turning behaviours. (**D**) Percentage of time where overlap in activity between segments exists for pre-application, application, and post-application of TA across all concentration ranges. (**Ei**) Percentage of time where there is activity in at least one segment for pre-application, application, and post-application of TA across all concentration ranges. Note the concentration-dependent reduction in total activity within the wash period. (**Eii**) The effect of

483 relative promotion (green) or suppression (red) of activity during TA application against the percentage of time
484 where there is activity in at least one segment post TA application. Note the absence of a bifurcation or trend
485 between wash activity and TA's promotive or suppressive activity relative to pre-application. (**Eiii**) Non-significant
486 relationship between the % overlap induced by TA and post-application silence. (**Eiv**) The relationship between
487 overall pre-application fictive activity ("Saline Activity") and the change in overall fictive activity during TA application
488 ("TA vs Saline"). Note the activity-dependent inhibitory effect of tyramine. Significant post-hoc comparisons are
489 exclusively shown denoted by ☐ saline vs wash, ✱ saline vs TA, Δ TA vs wash.

490 ## *Tdc*$^{2+}$ Neurons are Necessary and Sufficient for Fictive Locomotor Activity

491 Intrinsic *tdc*$^{2+}$ activity is highly correlated to segmental motor neuron activity with exogenous OA and
492 TA application modulating motor competition. We next evaluated if manipulating intrinsic *tdc*$^{2+}$ system
493 activity can also induce fictive motor bias, anterior asymmetric circuits potentiation post-application,
494 and alter motor competition. We expressed either *CsChrimson* or *GtACR1* in *tdc*$^{2+}$ neurons to
495 optogenetically manipulate the intrinsic adrenergic-like system and evaluate motor neuron activity
496 using nerve-root electrophysiology. Here, we show how intrinsic *tdc*$^{2+}$ activity is necessary and
497 sufficient for fictive locomotor activity and exhibits most of the phenotypic effects displayed by
498 exogenous OA application.

499 Firstly, we optogenetically depolarised *tdc*$^{2+}$ neurons by persistent red-light illumination (10, 20, 40s)
500 and recorded motor root activity from T3 and A6 VNC ganglia (Figure 4A). Optogenetic depolarisation
501 of *tdc*$^{2+}$ neurons induced significantly increased motor root bursting for all: 10s (pre: 9.6$\pm$7.5 m^{-1}, on:
502 55.4$\pm$26.1 m^{-1}, p = .002), 20s (pre: 11.4$\pm$4.6 m^{-1}, on: 46.3$\pm$9.1 m^{-1}, p=.002), and 40s (pre: 11.2$\pm$6.6 m^{-}
503 ^{1}, on: 41.0$\pm$12.9 m^{-1}, p=.005) stimulation periods (Figure 4A, Ci). The increased bursting frequency in
504 A6 was accompanied by significant decrease in bursting duration for all: 10s (pre: 2.8$\pm$1.3 m^{-1}, on:
505 1.0$\pm$0.4 m^{-1}, p=.002) 20s (pre: 3.3$\pm$1.2 m^{-1}, on: 0.9$\pm$0.3 m^{-1}, p=.004), and 40s (pre: 3.2$\pm$1.7 m^{-1}, on:
506 1.7$\pm$1.9 m^{-1}, p=.005) stimulation periods (Figure 4Cii). Elevated A6 motor root bursting frequency was
507 also evocable by pulsed-based stimulation (Supplementary Figure 4). Across both continuous and
508 pulsed-based stimulation of *tdc*$^{2+}$ neurons, intrinsic manipulation of the *tdc*$^{2+}$ system induced fictive
509 forward bias akin to results demonstrated by exogenous OA application (Figure 4E). Specifically,
510 optogenetic depolarisation of *tdc*$^{2+}$ neurons induced significantly increased fictive forward motor bias
511 for all: 10s (pre: 3.3$\pm$2.2 m^{-1}, on: 64.2$\pm$43.0 m^{-1}, p < .001), 20s (pre: 4.3$\pm$4.0 m^{-1}, on: 36.3$\pm$7.7 m^{-1}, p
512 < .001), and 40s (pre: 4.8$\pm$5.1 m^{-1}, on: 36.8$\pm$10.8 m^{-1}, p <.001) stimulation periods. In terms of fictive
513 bias, averaged across stimulation periods, optogenetic depolarisation of *tdc*$^{2+}$ neurons induced fictive
514 forward waves to become 79$\pm$8% of all fictive activity events during stimulation as opposed to
515 36$\pm$13% before or 36$\pm$14% after red-light stimulation.

516 Counter to the linear frequency relationship found between promoted fictive forward and anterior
517 asymmetric elevated activity post-application in exogenous octopamine application, anterior
518 asymmetric fictive activity was not elevated in the post-stimulation relative to pre-stimulation period
519 (Figure 4F). Further, while we witnessed a seemingly consistent elevation in silence (i.e., continuous
520 lack of apparent rhythmic activity in any nerve root) post optogenetic stimulation (see Figure 4A, ~40s
521 post-stimulation, 34.6$\pm$27.8 m) compared to control preparations (9.9$\pm$9.1 m), the duration of silence
522 did not significantly differ (p = .58) nor covary with stimulation period (10s: p = .07; 20s: p = .27; 40s:
523 p = .25) (Figure 4G).

524 Secondly, we optogenetically hyperpolarised *tdc*$^{2+}$ neurons with pulses of light (15s, 30s, 60s) and
525 recorded motor root activity from T3 and A6 VNC ganglia (Figure 4B). Optogenetic hyperpolarisation
526 of *tdc*$^{2+}$ neurons significantly reduced, and in many cases, completely collapsed, motor root bursting
527 for all light-stimulation periods: 15s (pre: 1.6$\pm$2.1 m^{-1}, on: 0.5$\pm$1 m^{-1}, p = .04), 30s (pre: 1.8$\pm$1.8 m^{-1},
528 on: 0$\pm$0 m^{-1}, p=.009), and 60s (pre: 2.2$\pm$2.1 m^{-1}, on: 0.4$\pm$0.7 m^{-1}, p = .01) illumination periods with 37
529 of 49 (75.9$\pm$30.8%) trials across preparations (N=7) showing no fictive activity during the white-light
530 stimulation period (Figure 4Bii, D). For longer period white-light stimulation (> 15s), there was weak
531 recovery of rhythmic activity in the A6, indicative of post-inhibitory rebound. Interestingly, long-lasting
532 (60s) white-light illumination in *tdc*$^{2+}$*>GtACR1* no retinol control preparations induced significantly
533 increased (pre: 1.8$\pm$2.0 m^{-1}, on: 3.7$\pm$1.5 m^{-1}, p = .01) A6 motor root activity potentially indicative of
534 photoreceptor-based motor stimulation in the isolated VNC preparation.

535 Thus, *tdc*$^{2+}$ depolarisation provokes elevated fictive forward activity akin to exogenous OA application.
536 Further, *tdc*$^{2+}$ hyperpolarisation collapsed all motor rhythms. Considering the strong correlation
537 between intrinsic *tdc*$^{2+}$ and motor neuron activity, such results demonstrate *tdc*$^{2+}$ neurons are
538 necessary and sufficient for fictive motor activity in isolated VNC 3rd *Drosophila* larval preparations.

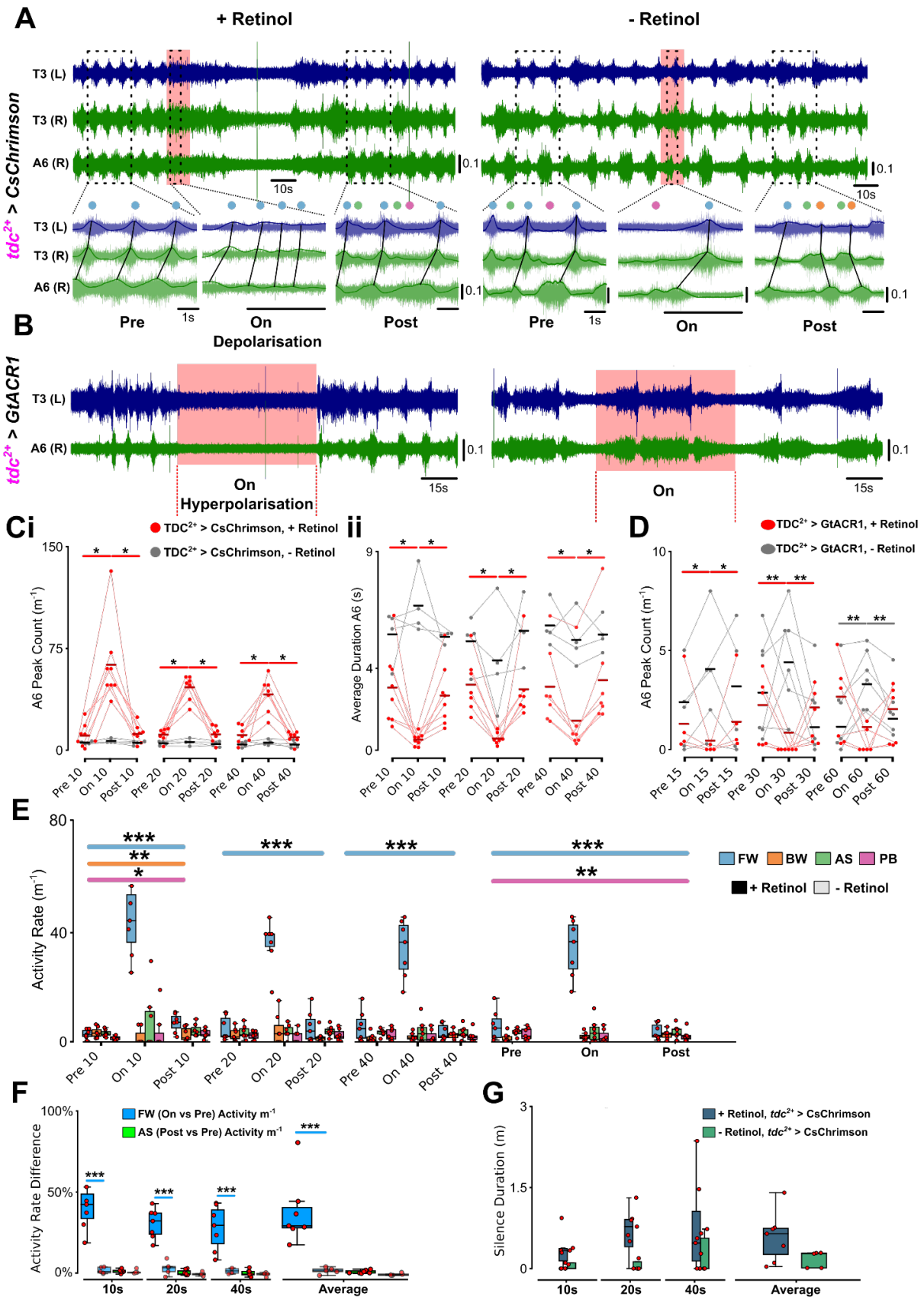

Figure 4: *tdc*$^{2+}$ Neuronal Activity is Sufficient and Necessary for Fictive Locomotor Activity

(**A**) Exemplar three nerve root (T3 (L), T3 (R), A6(R)) electrophysiology trace for continuous red-light depolarisation of *tdc*$^{2+}$ neurons using CsChrimson for preparations raised on retinol (experimental, left) and no retinol (control,

right). Before, during (red box), and post-stimulation periods are shown with rectified and smoothed traces shown. Black lines represent fictive activity motifs. (**B**) Exemplar two nerve root (T3 (L), A6 (R)) electrophysiology trace for continuous white-light hyperpolarisation (red box) of *tdc*$^{2+}$ neurons using GtACR1 for preparations raised on retinol (experimental, left), and no retinol (control, right). (**C**) Quantification of abdominal (A6) motor root bursting for (**i**) burst rate and (**ii**) duration of bursts in *tdc*$^{2+}$>CsChrimson for 10s, 20s, and 40s depolarisation period. (**D**) Quantification of abdominal (A6) motor root bursting for burst rate in *tdc*$^{2+}$>GtACR1 for 15s, 30s, and 60s hyperpolarisation period. (**E**) Change in the fictive activity profile for *tdc*$^{2+}$>CsChrimson stimulation periods demonstrating inducing of fictive forward bias across stimulation period. Activity profile within stimulation periods and average across stimulation periods are shown. (**F**) Difference in activity rate of fictive forward activity between stimulation and pre-stimulation period (blue) as well as fictive anterior asymmetric activity between post-stimulation and pre-stimulation period (green). (**G**) Duration of no rhythmic activity quantified post stimulation periods in control (- retinol) and experimental (+ retinol, CsChrimson) preparations. Comparisons followed by post-hoc was conducted with p-values: < .5 (*), < .01 (**), <.001 (***) shown. Only statistically significant bars are shown.

Given *tdc*$^{2+}$ VNC neurons are spatially segregated into each thoracic and abdominal ganglion, we next turned to see if spatially-restricted *tdc*$^{2+}$ activity may differentially modulate fictive locomotion network behaviour. To evaluate any effect of spatially-restricted release of OA on fictive locomotion, we performed restricted red-light stimulation on *tdc*$^{2+}$ neuronal populations in the ventromedial axis on the isolated ventral nerve cord. Qualitatively, direct red-light stimulation of *tdc*$^{2+}$ neuronal populations induces elevated bursting rate in all restricted regions: SOG (Figure 5A), thoracic ganglion (Figure 5B), anterior abdominal ganglion (Figure 5C), and posterior abdominal ganglion (Figure 5D). Across all stimulation regions, both the thoracic and abdominal nerve root bursting rate is significantly increased during *tdc*$^{2+}$ depolarisation (Figure 6Ai - Di). Specifically, direct SOG *tdc*$^{2+}$ depolarisation induced a significant increase in T3 (pre: 8.3$\pm$4.8 m^{-1}, on: 30.0$\pm$6.9 m^{-1}, p = .001) and A6 (pre: 8.8$\pm$4.7 m^{-1}, on: 31.7$\pm$10.8 m^{-1}, p = .001) motor root burst rate (Figure 6Ai). Direct thoracic ganglion (T1-3) *tdc*$^{2+}$ depolarisation induced a significant increase in T3 (pre: 6.5$\pm$3.4 m^{-1}, on: 30.0$\pm$6.0 m^{-1}, p < .001) and A6 (pre: 6.8$\pm$3.5 m^{-1}, on: 37.7$\pm$13.3 m^{-1}, p < .001) motor root burst rate (Figure 6Bi). Direct anterior abdominal ganglion (A1-3) *tdc*$^{2+}$ depolarisation induced a significant increase in T3 (pre: 6.6$\pm$2.1 m^{-1}, on: 34.3$\pm$12.4 m^{-1}, p = .001) and A6 (pre: 6.8$\pm$3.5 m^{-1}, on: 32.6$\pm$17.3 m^{-1}, p = .022) motor root burst rate (Figure 6Ci). Finally, direct posterior abdominal ganglion (A6-8) *tdc*$^{2+}$ depolarisation induced a significant increase in T3 (pre: 6.1$\pm$2.5 m^{-1}, on: 48.0$\pm$12.0 m^{-1}, p < .001) and A6 (pre: 6.5$\pm$2.1 m^{-1}, on: 45.4$\pm$9.7 m^{-1}, p < .001) motor root burst rate (Figure 6Di). Further, across all stimulation regions, both the thoracic and abdominal nerve root bursting duration was significantly reduced during *tdc*$^{2+}$ depolarisation with the exception of the T3 motor root during thoracic and anterior abdominal ganglion (Figure 6Ai-Di). Specifically, direct SOG *tdc*$^{2+}$ depolarisation induced a significant decrease in T3 (pre: 3.0$\pm$1.3s, on: 1.5$\pm$0.6s, p = .01) and A6 (pre: 3.0$\pm$1.3s, on: 1.3$\pm$0.4s, p = .03) motor root burst duration (Figure 6Ai). While direct thoracic ganglion (T1-3) *tdc*$^{2+}$ depolarisation did not induced a significant decrease in T3 motor root burst rate (pre: 2.9$\pm$1.0s, on: 1.5$\pm$0.4s, p = n.s),

depolarisation of T1-T3 *tdc*$^{2+}$ neurons did induce a significant decrease in the A6 motor root burst duration (pre: 3.1±1.9s, on: 1.4±0.6s, p = .02) (Figure 6Bi). While direct anterior abdominal ganglion (A1-3) *tdc*$^{2+}$ depolarisation did not induced a significant decrease in T3 motor root burst rate (pre: 3.2±1.2s, on: 1.5±0.4 m^{-1}, p = n.s), depolarisation of A1-A3 *tdc*$^{2+}$ neuron did induce a significant decrease in the A6 motor root burst duration (pre: 3.1±1.9s, on: 1.4±0.6s, p = .04) (Figure 6Ci). Finally, direct posterior abdominal ganglion (A6-8) *tdc*$^{2+}$ depolarisation induced a significant decrease in T3 (pre: 3.5±1.3s, on: 1.1±0.2s, p = .001) and A6 (pre: 3.3±1.1s, on: 1.1±0.2s, p = .003) motor root burst duration (Figure 6Di). Thus, depolarisation of any ganglion *tdc*$^{2+}$ neuron subpopulation is sufficient to induce elevated motor activity in the isolated ventral nerve curve.

We next examined if sub-region restricted *tdc*$^{2+}$ neuron depolarisation induced fictive forward bias akin to our earlier results on exogenous OA application and whole-VNC *tdc*$^{2+}$ depolarisation. Depolarisation of *tdc*$^{2+}$ neurons in the SOG (Figure 6Aii), thoracic ganglion (Figure 6Bii) and anterior abdominal ganglion (Figure 6Cii) induced an, albeit insignificant, elevated mixture of fictive behavioural patterns. However, decomposing the population data down into individual iterations of restricted stimulation across preparations did demonstrate a significant variation in the fictive bias within each region of *tdc*$^{2+}$ depolarisation (Supplementary Figure 5). Namely, restricted *tdc*$^{2+}$ depolarisation in the SOG (Supplementary Figure 5A, $\chi^2(2) = 7.3$, p = .007), thoracic ganglion (Supplementary Figure 5B, $\chi^2(2) = 7.3$, p = .007), and anterior abdominal ganglion (Supplementary Figure 5C, $\chi^2(2) = 7.3$, p = .007) all significant induced changes in fictive wave bias with some instances showing promotion of fictive forward whereas others fictive backward normalised bias. In other words, while averaging between preparations demonstrates a general trend of promoting both fictive forward and backward preparation in restricted *tdc*$^{2+}$ depolarisation in the SOG, T1-3, and A1-3, in individual trials, there are many instances of either fictive forward or backward bias resultants. In contrast, posterior abdominal restricted *tdc*$^{2+}$ depolarisation induced a significant increase in exclusively fictive forward motor activity (pre: 2.4±1.9m^{-1}, on: 38.6±13.8m^{-1}, p = .005) (Figure 6Dii). While posterior abdominal restricted *tdc*$^{2+}$ depolarisation similarly induced increased fictive bias variation (Supplementary Figure 5D, $\chi^2(2) = 5.8$, p = .02), a majority of stimulation instances were fictive forward biased. Thus, both abdominal posterior and whole *tdc*$^{2+}$ depolarisation induced locomotor CPGs into a fictive forward bias.

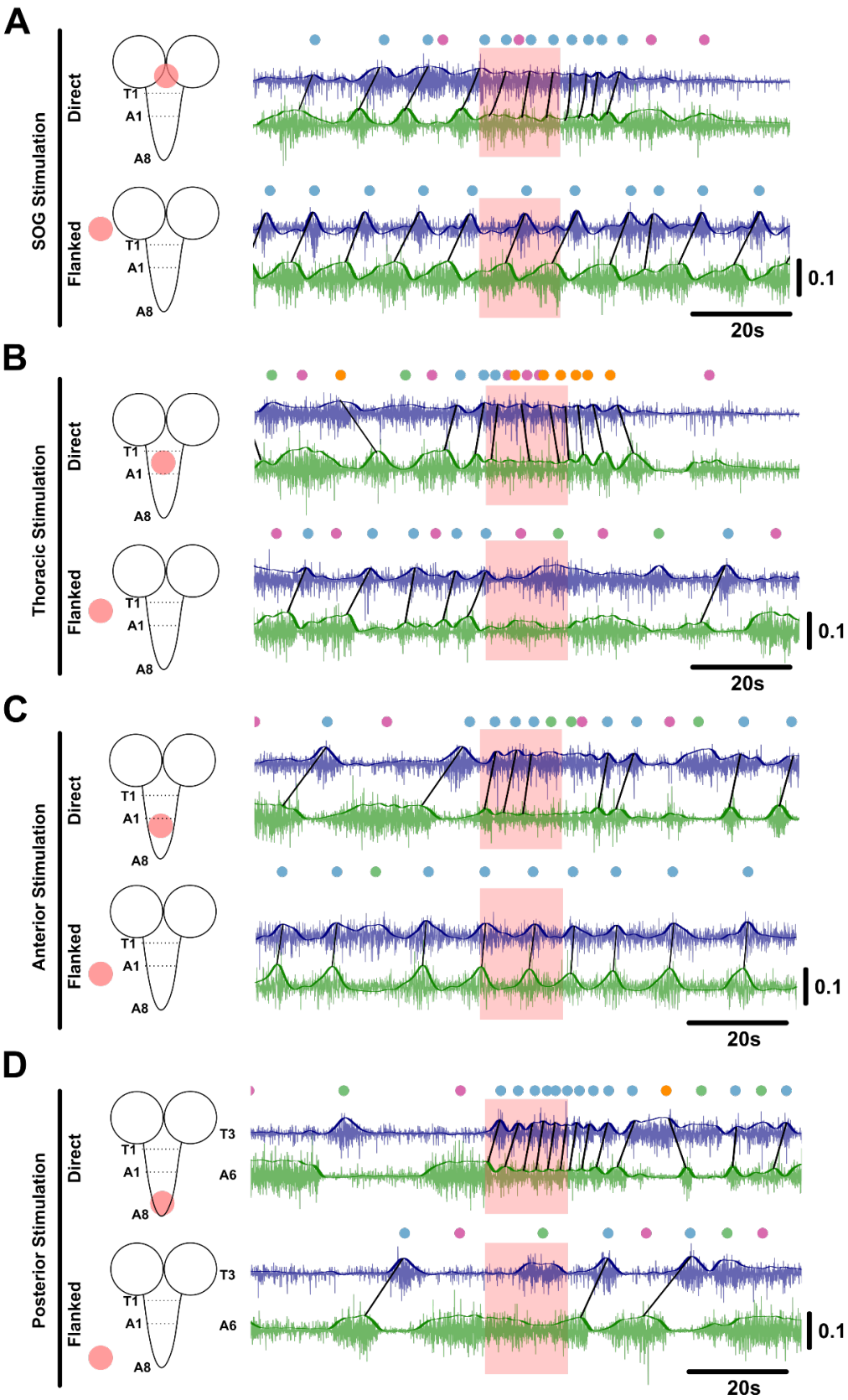

Figure 5: Restricted Optogenetic Stimulation of *tdc*$^{2+}$ Neurons Induces Diversity of Activity

Restricted 10s optogenetic stimulation of *tdc2+* neurons in the (**A**) SOG, (**B**) thoracic ganglion (T1-T3), (**C**) anterior abdominal ganglion (A1-A3), and (**D**) posterior abdominal ganglion (A6-A8). Representative electrophysiology

thoracic (T3) and posterior abdominal (A6) nerve root recording traces for direct and flanked stimulation conditions shown with coloured-dots indicating occurrence of fictive motor pattern: fictive forward wave (blue dot), posterior burst (purple dot), fictive backward wave (orange dot), anterior a/symmetric activity (green dot).

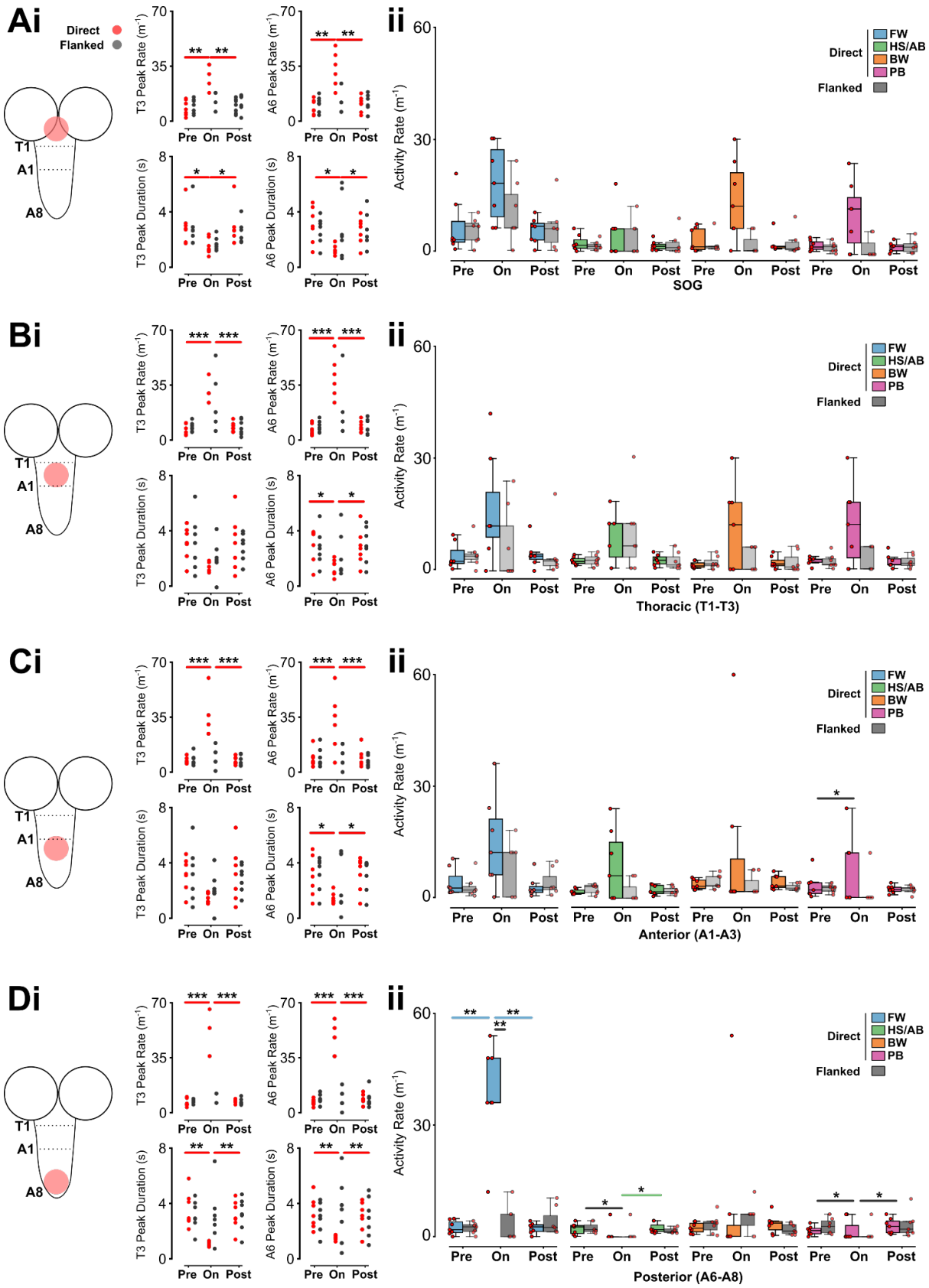

617 **Figure 6: Optogenetic Stimulation of Posterior Abdominal *tdc*$^{2+}$ Neurons Induces Fictive Forward**
618 **Locomotion**
619 Quantification of (**i**) abdominal and thoracic burst rate, burst duration, and (**ii**) fictive activity ("FW" = fictive forward
620 wave, "HS/AB" = anterior symmetric or asymmetric, "BW" = fictive backward wave, "PB" = posterior bust) rate
621 during direct (colour) and flanked (gray) optogenetic stimulation of (**A**) SOG, (**B**) thoracic ganglion (T1-T3), (**C**)
622 anterior abdominal ganglion (A1-A3), and (**D**) posterior abdominal ganglion (A6-A8) *tdc*$^{2+}$ neurons. Comparisons
623 followed by post-hoc was conducted with p-values: < .5 (*), < .01 (**), <.001 (***) shown. Only statistically significant
624 bars are shown.

625 Discussion

626 The adrenergic-like system is involved in a diversity of behaviours across invertebrates. Here, we show
627 that the adrenergic-like system is necessary and sufficient for generating rhythmic activity in
628 *Drosophila* larval CPG networks. Through acute manipulations to OA and TA signalling, we
629 demonstrate that the core adrenergic-like neuromodulators – OA and TA – may not always be
630 mutually-antagonistic for locomotion in *Drosophila* larvae. Finally, we discovered that a by-product
631 of extensive and sustained motor bias is an instantiation of antagonistic fictive activity after the end
632 of a prior bias episode. The crucial element of sustained movement is action selection and the
633 inhibition of competing motor programs. Here, we show how the isolated neural system appears to
634 have an innate disposition to rebalance motor diversity to antagonistic motor patterns in response to
635 sustained suppression of motor diversity through sustained motor bias.

636 The Fundamental Role of *tdc*$^{2+}$ Activity in *Drosophila* Larvae Fictive Activity

637 The cellular architecture of adrenergic-like *tdc*$^{2+}$ system in *Drosophila* is reported [45], [61] but the
638 broad functional role of the intact system, divorced from the inferences about the role of their
639 released neuromodulators, is less explored. Here, we showed how depolarisation of both the whole,
640 and subparts of, *tdc*$^{2+}$ system does drive fictive locomotion and how system-wide hyperpolarisation
641 collapses all rhythm generation in the isolated network.

642 Despite the absence of a comprehensive list of specific presynaptic partners for the *tdc*$^{2+}$ system, we
643 can infer that the *tdc*$^{2+}$ system likely exists directly upstream of the VNC rhythm generating networks.
644 Based on current connectomics data, only the ascending and descending subparts of the *Drosophila*
645 1st instar larva *tdc*$^{2+}$ system appear to have postsynaptic partners. The VNC *tdc*$^{2+}$ system - the vast
646 majority of our activity manipulation - appears to exclusively project to the neuromuscular junction
647 [45], [61], [62]. Given the high correlation in *tdc*$^{2+}$ system activity to system-wide segmental motor
648 activity alongside the fact that hyperpolarisation of the *tdc*$^{2+}$ system evoked an immediate cessation
649 of fictive activity, our results imply the *tdc*$^{2+}$ system may have a direct neuromodulatory roles that
650 might emerge after the 1st instar developmental stage. The complete connectome and architectural

651 makeup of the 3rd instar *Drosophila* larvae is undetermined; one testable prediction is that segmental
652 *tdc*$^{2+}$ neuronal populations are connected, directly or indirectly, to reported GDL/A27h premotor
653 circuity, or intermediary accessory of descending command neuronal structures like MDN, and Pair1
654 interneurons [63], [64], [65]. Further, the *tdc*$^{2+}$ system may make direct synaptic connections to
655 pacemaker command neurons (i.e., AcN, A01j) underpinning locomotory speed [66]. Indeed, such
656 predictions are supported by the tyraminergic architecture in *C. elegans* wherein the activity of RIM
657 neurons - presynaptic to GABAergic premotor neurons that facilitate bending - occurs prior to changes
658 in motor neuron activity [33], [48], [49], [50], [51]. Further, the highly coordinated and rhythmic
659 behaviour of the *tdc*$^{2+}$ system itself implies the existence of a similar intersegmental regulatory
660 architecture which may include GDL-like feedforward inhibitory motifs [64]. Importantly, the *tdc*$^{2+}$-
661 GAL4 construct also incorporates large ventral unpaired median (VUM) motor neurons - a subset of
662 the *tdc*$^{2+}$ system and motor neurons system - that appear to exclusively innervate the larval muscles
663 [63]. While hyperpolarizing these neurons should undoubtedly reduce motor pool activity, the fact
664 that system-wide motor activity comprehensively collapses under mass hyperpolarisation suggests
665 still a fundamental role of the interneuronal or descending portions of the *tdc*$^{2+}$ system in fictive
666 rhythmic generation. Consequently, we might expect any realised or modelled architecture of the
667 *tdc*$^{2+}$ system to incorporate a subpopulation motif for both internal and projecting outputs. Finally,
668 independent of architecture, the mechanism of modulation by the *tdc*$^{2+}$ system may be more complex
669 than simply adrenergic-like modulation by OA and TA exclusively. Indeed, we have only a partial OA/TA
670 receptor expression map restricted to the tissue, but not cellular level [4], [6], [67], [68]. Given that
671 different OA/TA receptor isoforms have fundamentally different downstream signalling effects [4] and
672 thus different effects on behaviour (e.g., [22]), any neuromodulatory mechanistic picture currently
673 lacks a firm foundation. Further, given a majority of adult *tdc*$^{2+}$ neurons co-express OA and glutamate
674 [69] and some *tdc*$^{2+}$ neurons modulate through gap junctions (e.g., APL neurons in the MB [70]), a
675 complex, potentially degenerate, neuromodulatory picture may underpin the mechanism behind *tdc*$^{2+}$
676 system fictive modulation. Overall, we show that the *tdc*$^{2+}$ system could be considered at least part of
677 a necessary and sufficient motif for rhythm generation in locmotor networks.

678 Our study uses the isolated VNC removing dynamic re-afferent and sensory feedback. Prior studies
679 have extensively shown how genetic manipulations to the adrenergic-like system in a variety of
680 invertebrates induces dysrhythmic movement [4], [9], [27], [28].Leaving aside potentially
681 developmental compensatory effects, the fact that genetic ablation of the *tdc*$^{2+}$ system does not arrest
682 all movement in intact animals[33], whereas our results on hyperpolarisation in isolated networks do
683 collapse rhythmic generation, implies re-afferent or sensory modulation may be one source of
684 compensation in intact animals with dysfunctional *tdc*$^{2+}$ system.s In future, the isolated

685 CNSpreparation and consequent analysis pipelines [1], [47] could be used to interrogate if there are
686 specific *tdc*$^{2+}$ system deficits induced by genetic manipulations, further bridging our understanding
687 between intact and fictive locomotion.

688 **The Adrenergic-like System in Modulating Motor Competition**

689 Movement necessitates a balance between excitation-driven initiation of a rhythm and pattern
690 generating circuit alongside inhibition of competing motor program-related networks. Motor
691 competition - the dynamic interplay that underpins excitatory and inhibitory neural action - is one lens
692 through which the OA/TA modulatory dichotomy has yet to be examined. Here, we demonstrated that
693 the well-reported excitatory role of OA and the inhibitory role of TA can be considered as
694 neuromodulators underpinning motor network competition.

695 The locomotor effects of OA/TA neuromodulation are well-reported across a variety of invertebrate
696 species. Generally, the OA/TA are considered mutual-antagonistic in locomotor neuromodulation with
697 an excitatory/inhibitory binary [4], [26] .Complementing some studies that highlighted nuanced roles
698 for adrenergic-like neuromodulation [26], we showed that TA exhibited activity-dependent inhibitory
699 effects, was promotive of overlapping between fictive programs, thus not exclusively leading to
700 inhibitory effects. Thus, the slower and shorter locomotion exhibited when *Drosophila* larva are fed
701 TA [27] could be conceived as a failure to regulate motor competition rather than a direct, general
702 inhibitory effect. Those two competing explanations for TA effects are non-trivial differences. For
703 instance, while TA has a hyperpolarising effect on an isolated neuron [34] ,we found an overall trend
704 of TA to depolarise motor pool activity. Our indication that TA's inhibitory effects may be a product of
705 activity state can help marry the two bodies of thought. Namely, given that intrinsic *tdc*$^{2+}$ activity is
706 highly coupled to fictive motor activity, *tdc*$^{2+}$ activity is indicative of OA release [45], and that TA's
707 effects might be conditional on OA levels [26], one can see how TA/OA's antagonism is in response to
708 their neuromodulatory effects. At a functional level, we therefore could consider OA/TA as mutual-
709 antagonists altering motor competition rather than generally activity levels.

710 Our results and the role of the *tdc*$^{2+}$ system in *Drosophila* larvae can be greatly contextualised by its
711 similarity to the *C. elegans* neuroarchitecture underpinning turning escape behaviour. Within *C.*
712 *elegans*, OA/TA play a significant and fundamental role in modulating escape behaviour and motor
713 competition through the AVA/AVB/RIM motif [26], [50]. Importantly, the proposed motif
714 demonstrates how TA/OA underpins motor competition between spontaneous forward and backward
715 locomotion through TA's disinhibition [51]. Taken together with the effect of increased overlap and
716 activity-dependent inhibition within our work, we could expect TA to have a similar disinhibitory role

717 in *Drosophila*. Namely, as reported in our recent work [1], core interneuronal inhibitory motifs might
718 be essential for all forms of motor selection and appropriate rhythmic output. Thus, we would expect
719 the *tdc*$^{2+}$ system - itself releasing neuromodulators essential for escape responses - to be integral to
720 orchestrating and modulating the dynamics of motor selection at a fundamental level.
721
722 OA's excitatory effect on fictive motor behaviour is reflective of an underlying inhibition of motor
723 competition. Reminiscent of a large catalogue of prior studies [3], [8], [9], [26], [27], [32], we found
724 exogenously-applied OA was excitatory by being promotive of forward fictive locomotion with higher
725 intersegmental propagation of activity. Importantly, this promotion of locomotion, especially given
726 the network appeared perpetually active with little to no episodes of non-activity, was reflective of
727 significant inhibition of competing motor program occurrence. Indicative of a suppression of initiation,
728 we here contextualise the neuromodulator OA, in comparison to TA, as a suppressor of motor
729 competition. Reflective of a deeper role of the adrenergic-like system in motor competition, the
730 emergence of proportional post-application activity changes due to OA's neuromodulatory effects
731 indicates a potential foundational connection in CPG competition. Given that asymmetric anterior
732 activity can be considered a preliminary and important element of backward locomotion [1], the fact
733 OA's induction of an exclusive fictive forward bias precipitated an elevation of such asymmetric
734 anterior activity post-hoc suggests a potential underpinning dynamic in motor selection. Namely, a
735 long-lasting memory-like system may exist to compensate for extremes in fictive forward activity that
736 compensates if that extreme bias manifests. Indeed, the emergence of post-application elevation in
737 silence from TA perfusion may also be reflective of a long-lasting effect to motor competition
738 promotion. Unsurprisingly, inhibition is a vital element in necessitating variability as for a system to
739 be able to devolve into different output modes it must first have a configuration that allows it to sit at
740 that potential junction (i.e., conception of criticality) [1], [71]. Notably, there was no apparent post-
741 asymmetric elevation in our electrophysiology-based stimulation as exhibited in our exogenous
742 perfusion data. Thus, we would predict "long-lasting bias" could be denoted within a motor system as
743 dominance of one fictive motif beyond a 60s episode.

744 Taken together, here we provide a case of how the *tdc*$^{2+}$ system in *Drosophila* may be a necessary and
745 sufficient component in rhythm generation underlying locomotion. Further, we nuance the role of
746 adrenergic-like neuromodulation in motor competition by demonstrating how OA/TA operate to
747 either restrain or promote diversity of fictive motor programmes. Our results provide constraints on
748 modelling studies and a framework for further connectomics exploration into how the *tdc*$^{2+}$ activity is
749 integrated into the pre-motor system. Finally, we highlight a novel potential relationship within motor

750 competition between induced locomotion bias and long-lasting fictive antagonism that may
751 demonstrate a fundamental relationship of CPG networks not currently considered.

752 Conflicts of Interest

753 No declared conflict of interest.

754 Data Avaliability

755 The research data supporting this publication can be accessed at https://doi.org/10.17630/84df17ac-
756 77d3-4a61-9bf0-fa6e78a802e1.

757 Author's Contribution

758 S.R.P. and W.V.S. conceived the study. W.V.S conducted all experiments, analysis, and visualisation.
759 W.V.S. and S.R.P finalised the figures. S.R.P. supervised the project.

760 Acknowledgements

761 This project was made possible by an Industrial CASE PhD studentship (UKRI Biotechnology and
762 Biological Sciences Research Council (BBSRC) grant number BB/T00875X/1) to W.V.S.

Supplementary Figures

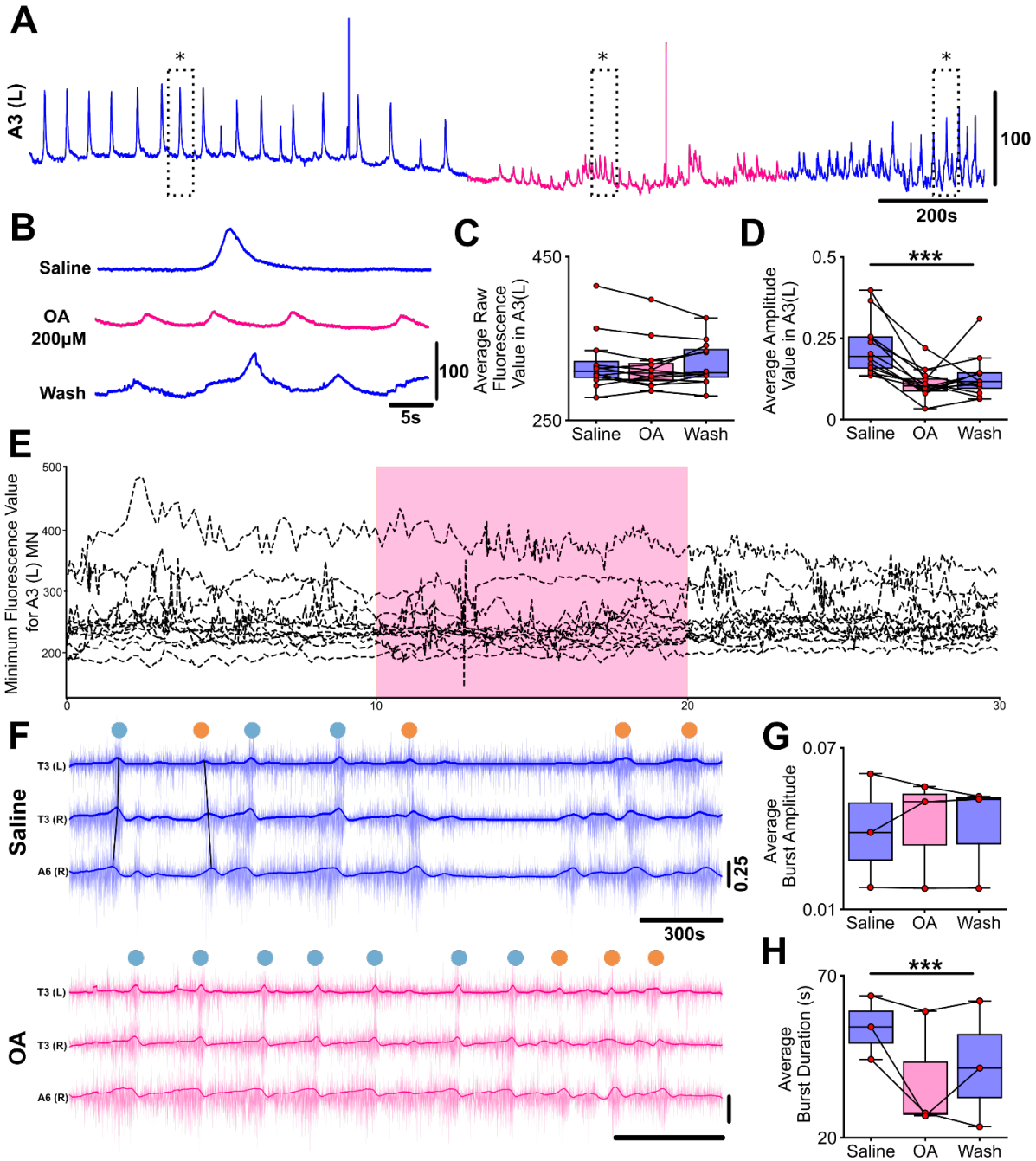

Supplementary Figure 1: Octopamine Decreases Calcium Signal Amplitude and Motor Root Burst Duration Despite No Baseline Change

(**A**) Representative calcium signal trace from A3 left motor neuron before (blue), during 200μM octopamine application (magenta), and after (blue). (**B**) Exemplar activity in the left A3 calcium signal before, during 200μM octopamine application and after. Traces in B are subsections of the total trace denoted by *. (**C**) The average fluorescence value from calcium signal trace before, during, and after 200μM octopamine application. (**D**) The averaged peak amplitude from all A3 motor neuron calcium activity from calcium signal trace before, during, and after 200μM octopamine application across full ventral nerve cord (VNC) perfusion experiments (N=12). (**E**) All traces from full VNC perfusion experiments (grey, dashed line) before, during (magenta box), and after 200μM octopamine application. Note the absence of a visual change in baseline during octopamine application (magenta

box). (**F**) Nerve root recordings for full VNC before (blue) and during (magenta) 200µM octopamine bath application. Yellow lines indicate fictive patterns. Note the elevated frequency of fictive forward wave activity during octopamine application (yellow lines, magenta traces). (**G**) The average amplitude of peaks in A6 motor neurons before and after 200µM octopamine application (N=3). (**H**) The average burst duration of peaks in A7 motor neurons before and after 200µM octopamine application (N=3). Note, the decreased burst duration in motor activity represents calcium activity as a lower signal amplitude. Post-hoc comparison were conducted with p-values: < .5 (*), < .01 (**), <.001 (***) shown. Only statistically significant bars are shown.

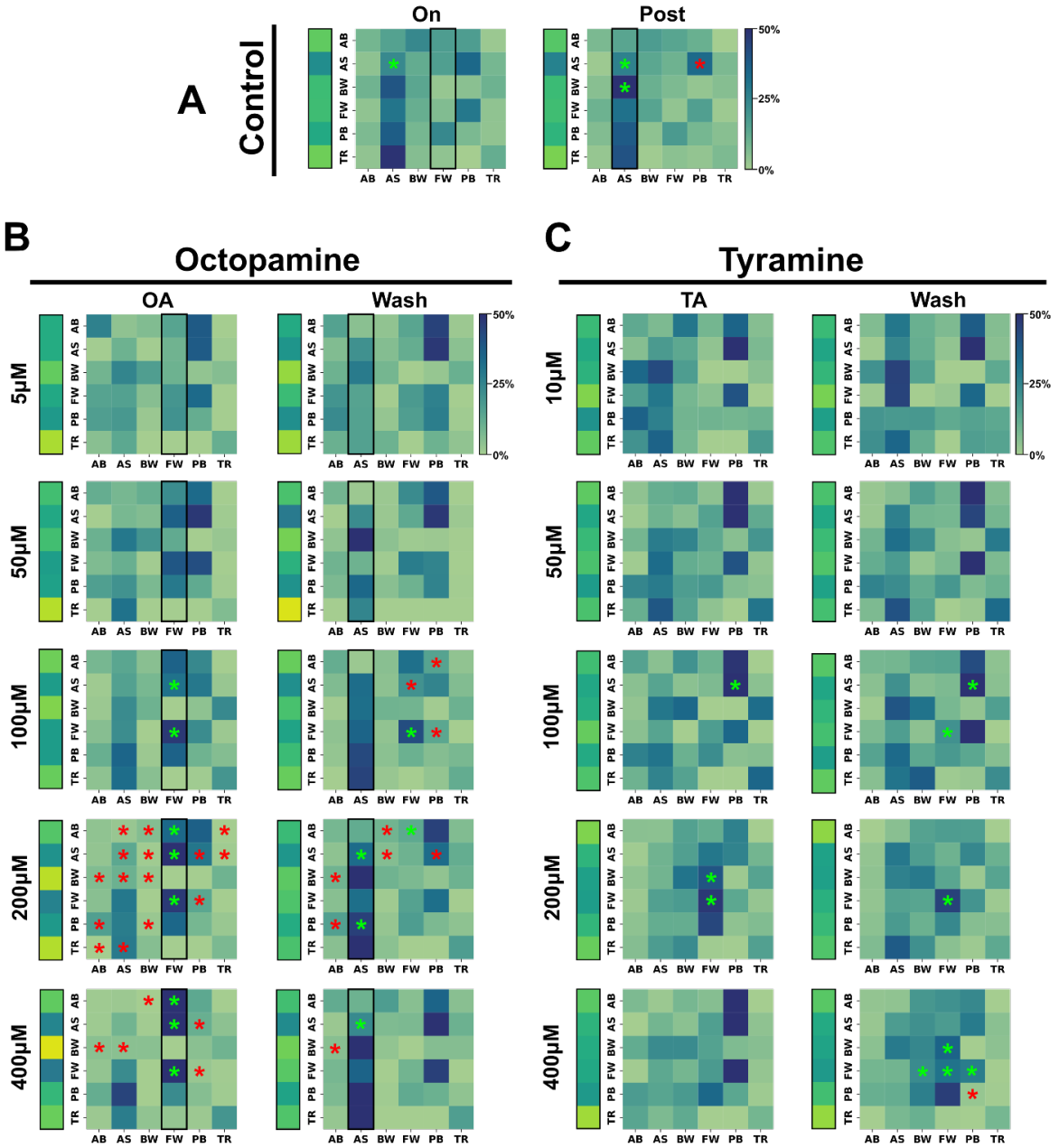

Supplementary Figure 2: Octopamine and Tyramine Alters Motor Competition by Modulation Fictive Transition Probabilities

(**A**) The probability of any fictive behavioural transition (column) to a subsequent fictive program (row) within OK371>GCaMP6m control data (N=28) within the 10 to 20 minute time period ("On") representative of the time period of the neuromodulator perfusion period and > 20 minute time period ("Post) representative of the time period of the neuromodulator wash period. "On" statistical comparisons made between the average transition probabilities

in the 10-20 minute period across all control isolated 3rd instar ventral nerve cords compared to the average transition probabilities in the 0-10 minute period. “Post” statistical comparisons are made between the average transition probabilities in the 20-30 minute period across all control data compared to the average transition probabilities in the 0-10 minute period. (**B**) The average fictive transition probabilities across all the octopamine (OA) concentrations within the application (“On”) and post-application (“Wash”) period. (**C**) The average fictive transition probabilities across all the tyramine (TA) concentrations within the application (“On”) and post-application (“Wash”) period. Post-hoc comparison were conducted with p-values: < .5 (*), < .01 (**), <.001 (***) shown. Only statistically significant bars are shown.

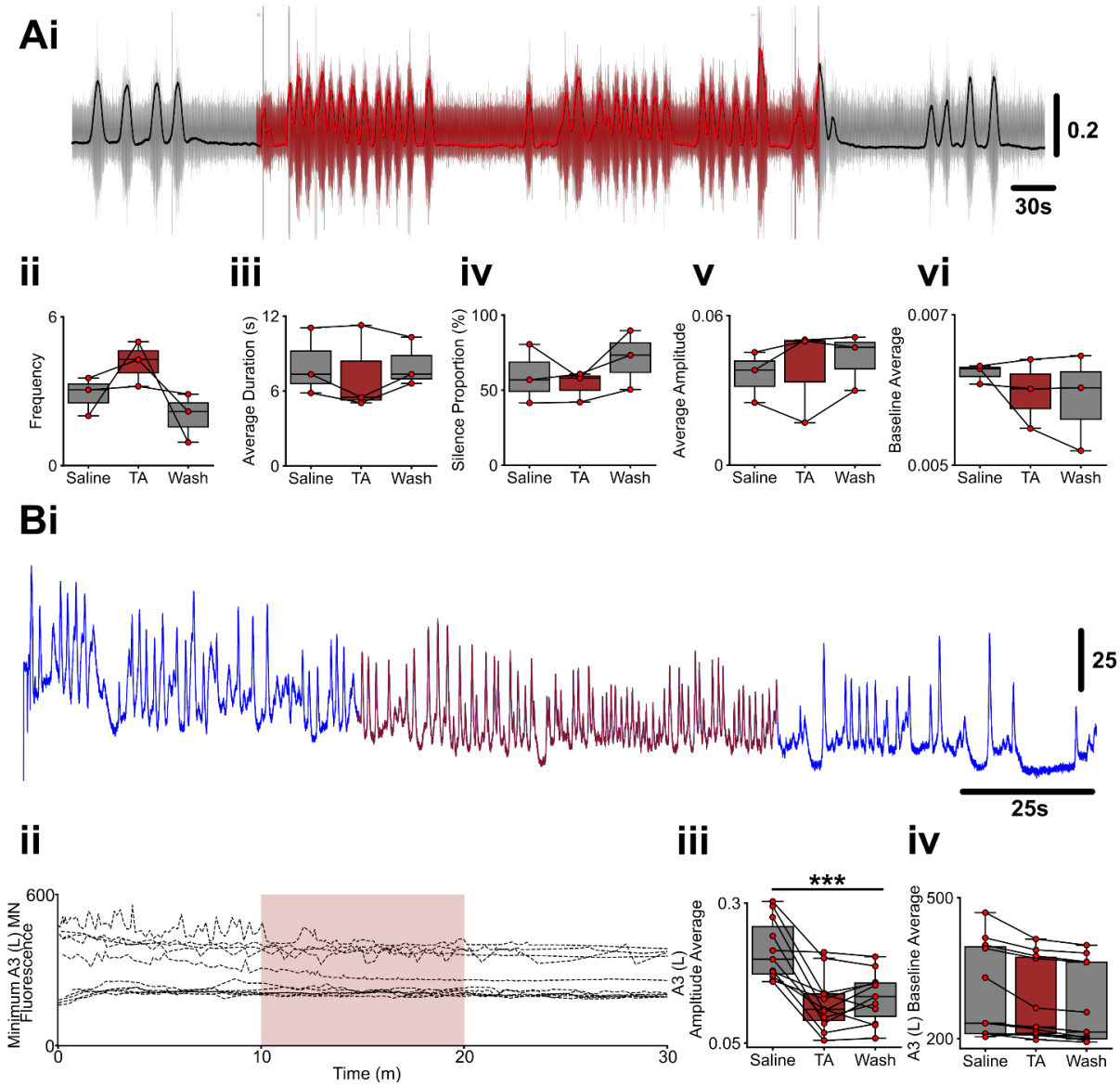

Supplementary Figure 3: Tyramine Shows No Inhibition of Motor Root Activity nor Calcium Baseline

(**A**) Effects of 50μM tyramine bath application on posterior abdominal motor nerve root activity demonstrating (**Ai**) subtle changes to firing patterns (N=3). The effect of 50μM tyramine bath application on posterior abdominal motor root (**Aii**) bursting frequency, (**Aiii**) average burst duration, (**Aiv**), proportion of time (%) without activity > 5% change from baseline, (**Av**) average burst amplitude, and (**Avi**) baseline average for the pre-application (“Saline”), application (“TA”), and post-application (“Wash”) periods. (**B**) Representative effects of 200μM tyramine bath application (dark red) (N=11) on the (**Bi**) calcium activity on the motor neuron pool (abdominal segment 3, left: A3 (L)). (**Bii**) The baseline calcium fluorescence for all isolated ventral nerve cord preparations under 200μM tyramine

807 bath application (dark red). The effect of 200μM tyramine bath application on (**Biii**) average calcium amplitude
808 across fictive programs and (**Biv**) baseline calcium signal. Post-hoc comparison were conducted with p-values: <
809 .5 (*), < .01 (**), <.001 (***) shown. Only statistically significant bars are shown.

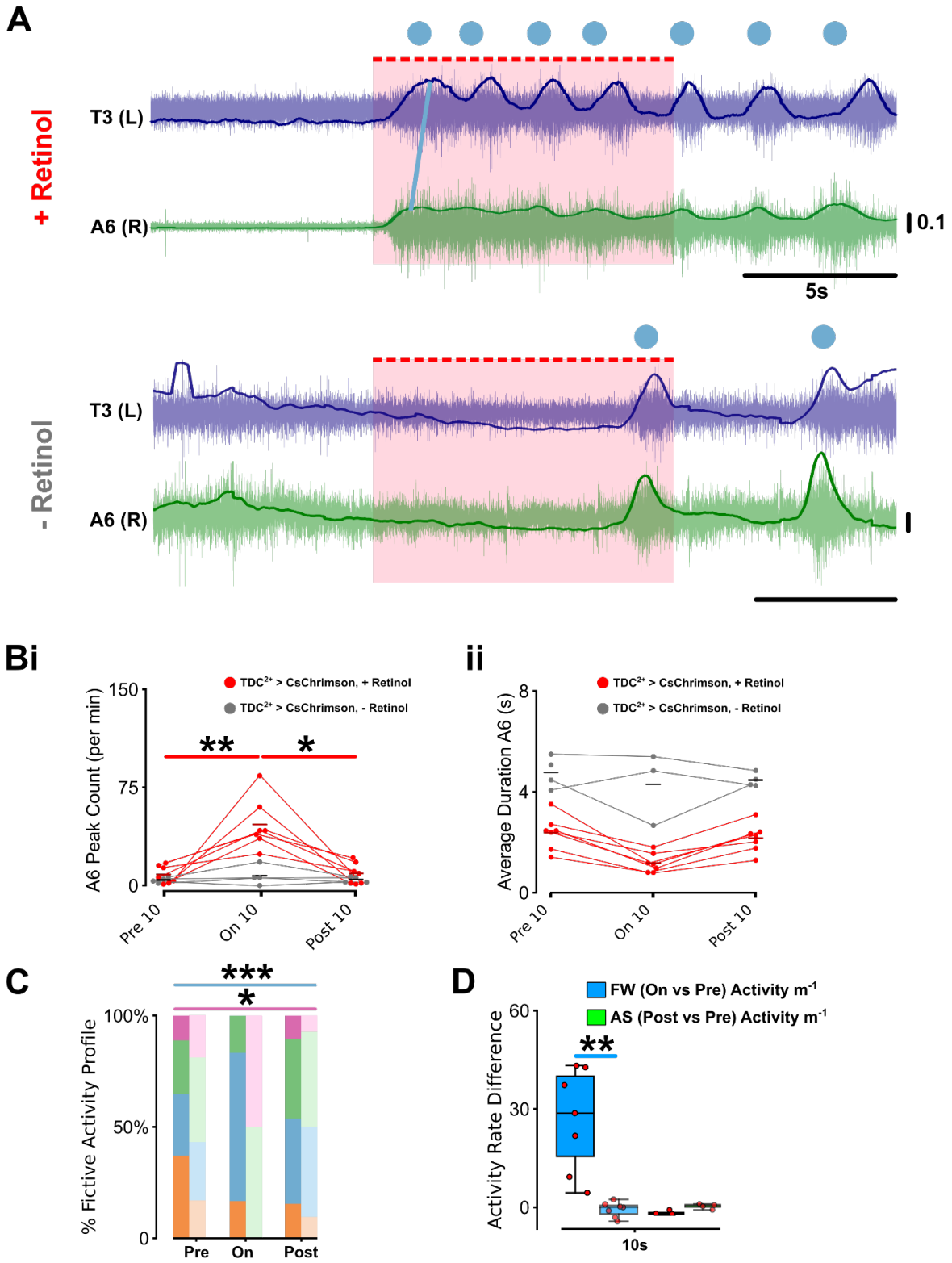

810
811

Supplementary Figure 4: Pulsed Stimulation of *tdc*$^{2+}$ Neurons Induces Fictive Forward Bias

(**A**) Representative T3(L) and A6(R) motor root electrophysiology trace demonstrating promotion of fictive forward activity during pulsed stimulation of CsChrimson>*tdc*$^{2+}$ (0.01s, 40Hz, 400 repeats = 10s total stimulation) for experimental (+ retinol) compared to control (- retinol) 3rd instar *Drosophila* larva. (**B**) Quantification of motor root bursting at A6 demonstrating (**i**) peak rate and (**ii**) burst duration changes upon pulsed stimulation (On10) relative to before (Pre10) and after (Post10) stimulation period. (**C**) Quantification of fictive bias before, during, and after pulsed stimulation in preparations where fictive activity could be accurately inferred (N=6). (**D**) The relative fictive activity difference for fictive forward activity during (on) vs before (pre) stimulation (blue) and for anterior asymmetric fictive activity after (post) vs before (pre) stimulation (green). Comparisons followed by post-hoc was conducted with p-values: < .5 (*), < .01 (**), <.001 (***) shown. Only statistically significant bars are shown.

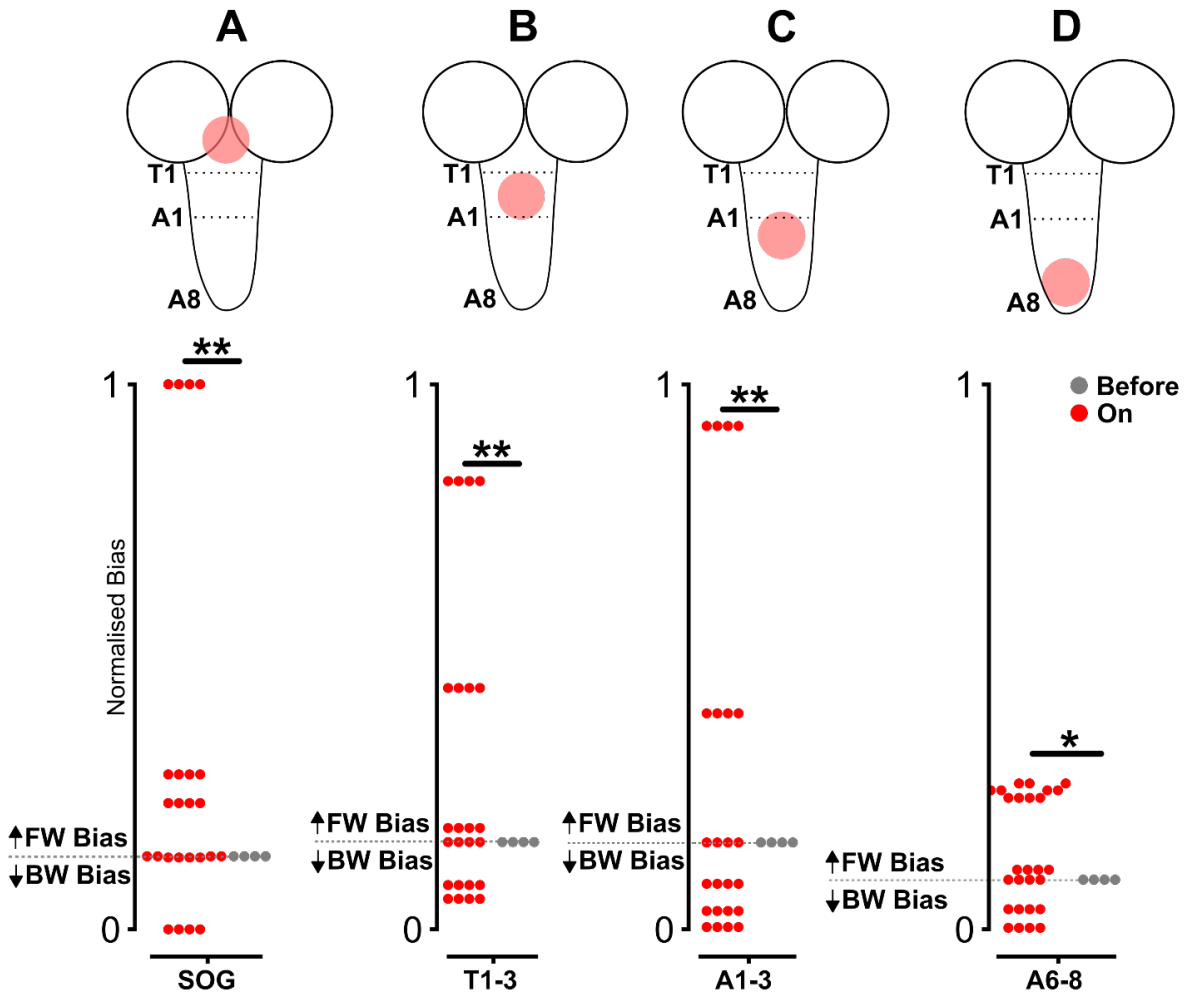

Supplementary Figure 5: Relative Fictive Wave Bias Induced by Restricted Stimulation of *tdc*$^{2+}$ Neurons

Restricted *tdc*$^{2+}$ depolarisation in the (A) SOG, (B), thoracic ganglion (T1-3), (C) anterior abdominal ganglion (A1-3), and (D) posterior abdominal ganglion (A6-8) induces different fictive wave bias in different stimulation periods (N > 2) across all preparations (N = 7). Plots show normalised bias of fictive forward activity rate (m^{-1}) / fictive backward activity rate (m^{-1}) with gray dashed line indicative of relative fictive wave bias before restricted stimulation. Note, across all stimulation periods there are a diverse array of bias changes (i.e., below the level of normalised bias before stimulation = more fictive backward wave bias, above the level of normalised bias before stimulation =

more fictive forward wave bias). Comparisons followed by post-hoc was conducted with p-values: < .5 (*), < .01 (**), <.001 (***) shown. Only statistically significant bars are shown.

References

[1] J. Francis *et al.*, 'Inhibitory circuit motifs in Drosophila larvae generate motor program diversity and variability', *PLOS Biol.*, vol. 23, no. 4, p. e3003094, Apr. 2025, doi: 10.1371/journal.pbio.3003094.

[2] T. Jovanic *et al.*, 'Competitive Disinhibition Mediates Behavioral Choice and Sequences in Drosophila.', *Cell*, vol. 167, no. 3, pp. 858-870.e19, Oct. 2016, doi: 10.1016/j.cell.2016.09.009.

[3] T. Roeder, 'The control of metabolic traits by octopamine and tyramine in invertebrates', *J. Exp. Biol.*, vol. 223, no. 7, p. jeb194282, Apr. 2020, doi: 10.1242/jeb.194282.

[4] T. Farooqui, 'Review of octopamine in insect nervous systems', *Open Access Insect Physiol.*, p. 1, Jun. 2012, doi: 10.2147/OAIP.S20911.

[5] Y. Pei, A. Asif-Malik, and J. J. Canales, 'Trace Amines and the Trace Amine-Associated Receptor 1: Pharmacology, Neurochemistry, and Clinical Implications', *Front. Neurosci.*, vol. 10, Apr. 2016, doi: 10.3389/fnins.2016.00148.

[6] M. Kutsukake, A. Komatsu, D. Yamamoto, and S. Ishiwa-Chigusa, 'A tyramine receptor gene mutation causes a defective olfactory behavior in Drosophila melanogaster', *Gene*, vol. 245, no. 1, pp. 31–42, Mar. 2000, doi: 10.1016/S0378-1119(99)00569-7.

[7] M. Monastirioti, M. Gorczyca, J. Rapus, M. Eckert, K. White, and V. Budnik, 'Octopamine immunoreactivity in the fruit fly *Drosophila melanogaster*', *J. Comp. Neurol.*, vol. 356, no. 2, pp. 275–287, May 1995, doi: 10.1002/cne.903560210.

[8] Y. Nagaya, M. Kutsukake, S. I. Chigusa, and A. Komatsu, 'A trace amine, tyramine, functions as a neuromodulator in Drosophila melanogaster', *Neurosci. Lett.*, vol. 329, no. 3, pp. 324–328, Sep. 2002, doi: 10.1016/S0304-3940(02)00596-7.

[9] M. Selcho, D. Pauls, B. El Jundi, R. F. Stocker, and A. S. Thum, 'The Role of octopamine and tyramine in *Drosophila* larval locomotion', *J. Comp. Neurol.*, vol. 520, no. 16, pp. 3764–3785, Nov. 2012, doi: 10.1002/cne.23152.

[10] M. Vömel and C. Wegener, 'Neuroarchitecture of Aminergic Systems in the Larval Ventral Ganglion of Drosophila melanogaster', *PLoS ONE*, vol. 3, no. 3, p. e1848, Mar. 2008, doi: 10.1371/journal.pone.0001848.

[11] T. Farooqui, 'Octopamine-Mediated Neuromodulation of Insect Senses', *Neurochem. Res.*, vol. 32, no. 9, pp. 1511–1529, Jul. 2007, doi: 10.1007/s11064-007-9344-7.

[12] M. Selcho, 'Octopamine in the mushroom body circuitry for learning and memory', *Learn. Mem.*, vol. 31, no. 5, p. a053839, May 2024, doi: 10.1101/lm.053839.123.

[13] S. C. Hoyer *et al.*, 'Octopamine in Male Aggression of Drosophila', *Curr. Biol.*, vol. 18, no. 3, pp. 159–167, Feb. 2008, doi: 10.1016/j.cub.2007.12.052.

[14] I. K. Yakovlev, 'Effects of Octopamine on Aggressive Behavior in Red Wood Ants', *Neurosci. Behav. Physiol.*, vol. 48, no. 3, pp. 279–288, Mar. 2018, doi: 10.1007/s11055-018-0561-0.

[15] P. A. Stevenson, V. Dyakonova, J. Rillich, and K. Schildberger, 'Octopamine and Experience-Dependent Modulation of Aggression in Crickets', *J. Neurosci.*, vol. 25, no. 6, pp. 1431–1441, Feb. 2005, doi: 10.1523/JNEUROSCI.4258-04.2005.

[16] K. Mizutani, H. Ogawa, J. Saito, and K. Oka, 'Fictive locomotion induced by octopamine in the earthworm', *J. Exp. Biol.*, vol. 205, no. 2, pp. 265–271, Jan. 2002, doi: 10.1242/jeb.205.2.265.

[17] I. Orchard, J. M. Ramirez, and A. B. Lange, 'A Multifunctional Role for Octopamine in Locust Flight', *Annu. Rev. Entomol.*, vol. 38, no. 1, pp. 227–249, Jan. 1993, doi: 10.1146/annurev.en.38.010193.001303.

[18] J. C. Ormshaw and C. J. H. Elliott, ‘Octopamine boosts snail locomotion: behavioural and cellular analysis’, *Invert. Neurosci.*, vol. 6, no. 4, pp. 215–220, Nov. 2006, doi: 10.1007/s10158-006-0031-1.

[19] T. Roeder, ‘TYRAMINE AND OCTOPAMINE: Ruling Behavior and Metabolism’, *Annu. Rev. Entomol.*, vol. 50, no. 1, pp. 447–477, Jan. 2005, doi: 10.1146/annurev.ento.50.071803.130404.

[20] D. J. Candy, ‘The regulation of locust flight muscle metabolism by octopamine and other compounds’, *Insect Biochem.*, vol. 8, no. 3, pp. 177–181, Jan. 1978, doi: 10.1016/0020-1790(78)90070-7.

[21] Y. Li *et al.*, ‘Octopamine controls starvation resistance, life span and metabolic traits in Drosophila’, *Sci. Rep.*, vol. 6, no. 1, p. 35359, Oct. 2016, doi: 10.1038/srep35359.

[22] A. C. Koon and V. Budnik, ‘Inhibitory Control of Synaptic and Behavioral Plasticity by Octopaminergic Signaling’, *J. Neurosci.*, vol. 32, no. 18, pp. 6312–6322, May 2012, doi: 10.1523/JNEUROSCI.6517-11.2012.

[23] A. C. Koon *et al.*, ‘Autoregulatory and paracrine control of synaptic and behavioral plasticity by octopaminergic signaling’, *Nat. Neurosci.*, vol. 14, no. 2, pp. 190–199, Feb. 2011, doi: 10.1038/nn.2716.

[24] Z. Yang, Y. Yu, V. Zhang, Y. Tian, W. Qi, and L. Wang, ‘Octopamine mediates starvation-induced hyperactivity in adult *Drosophila*’, *Proc. Natl. Acad. Sci.*, vol. 112, no. 16, pp. 5219–5224, Apr. 2015, doi: 10.1073/pnas.1417838112.

[25] A. Sujkowski, D. Ramesh, A. Brockmann, and R. Wessells, ‘Octopamine Drives Endurance Exercise Adaptations in Drosophila’, *Cell Rep.*, vol. 21, no. 7, pp. 1809–1823, Nov. 2017, doi: 10.1016/j.celrep.2017.10.065.

[26] B. Brembs, F. Christiansen, H. J. Pflüger, and C. Duch, ‘Flight Initiation and Maintenance Deficits in Flies with Genetically Altered Biogenic Amine Levels’, *J. Neurosci.*, vol. 27, no. 41, pp. 11122–11131, Oct. 2007, doi: 10.1523/JNEUROSCI.2704-07.2007.

[27] S. Saraswati, L. E. Fox, D. R. Soll, and C. Wu, ‘Tyramine and octopamine have opposite effects on the locomotion of *Drosophila* larvae’, *J. Neurobiol.*, vol. 58, no. 4, pp. 425–441, Mar. 2004, doi: 10.1002/neu.10298.

[28] L. E. Fox, D. R. Soll, and C.-F. Wu, ‘Coordination and Modulation of Locomotion Pattern Generators in *Drosophila* Larvae: Effects of Altered Biogenic Amine Levels by the Tyramine β Hydroxlyase Mutation’, *J. Neurosci.*, vol. 26, no. 5, pp. 1486–1498, Feb. 2006, doi: 10.1523/JNEUROSCI.4749-05.2006.

[29] H. Hashemzadeh-Gargari and W. Otto Friesen, ‘Modulation of swimming activity in the medicinal leech by serotonin and octopamine’, *Comp. Biochem. Physiol. Part C Comp. Pharmacol.*, vol. 94, no. 1, pp. 295–302, Jan. 1989, doi: 10.1016/0742-8413(89)90182-5.

[30] B. Johnson and R. Harris-Warrick, ‘Aminergic modulation of graded synaptic transmission in the lobster stomatogastric ganglion’, *J. Neurosci.*, vol. 10, no. 7, pp. 2066–2076, Jul. 1990, doi: 10.1523/JNEUROSCI.10-07-02066.1990.

[31] S. C. Kinnamon, L. W. Klaassen, A. E. Kammer, and D. Claassen, ‘Octopamine and chlordimeform enhance sensory responsiveness and production of the flight motor pattern in developing and adult moths’, *J. Neurobiol.*, vol. 15, no. 4, pp. 283–293, Jul. 1984, doi: 10.1002/neu.480150405.

[32] J. M. Ramirez and K. G. Pearson, ‘Octopaminergic modulation of interneurons in the flight system of the locust’, *J. Neurophysiol.*, vol. 66, no. 5, pp. 1522–1537, Nov. 1991, doi: 10.1152/jn.1991.66.5.1522.

[33] M. J. Alkema, M. Hunter-Ensor, N. Ringstad, and H. R. Horvitz, ‘Tyramine Functions Independently of Octopamine in the Caenorhabditis elegans Nervous System’, *Neuron*, vol. 46, no. 2, pp. 247–260, Apr. 2005, doi: 10.1016/j.neuron.2005.02.024.

[34] N. Schützler *et al.*, ‘Tyramine action on motoneuron excitability and adaptable tyramine/octopamine ratios adjust *Drosophila* locomotion to nutritional state’, *Proc. Natl. Acad. Sci.*, vol. 116, no. 9, pp. 3805–3810, Feb. 2019, doi: 10.1073/pnas.1813554116.

[35] B. Mulloney, L. D. Acevedo, and A. G. Bradbury, ‘Modulation of the crayfish swimmeret rhythm by octopamine and the neuropeptide proctolin’, *J. Neurophysiol.*, vol. 58, no. 3, pp. 584–597, Sep. 1987, doi: 10.1152/jn.1987.58.3.584.
[36] A. D. McClellan, G. D. Brown, and P. A. Getting, ‘Modulation of swimming in Tritonia: excitatory and inhibitory effects of serotonin’, *J. Comp. Physiol. A*, vol. 174, no. 2, Feb. 1994, doi: 10.1007/BF00193792.
[37] K. Nishikawa and Y. Kidokoro, ‘Octopamine inhibits synaptic transmission at the larval neuromuscular junction in Drosophila melanogaster’, *Brain Res.*, vol. 837, no. 1–2, pp. 67–74, Aug. 1999, doi: 10.1016/S0006-8993(99)01676-5.
[38] Z.-T. Zhu, A. C. Munhall, and S. W. Johnson, ‘Tyramine excites rat subthalamic neurons in vitro by a dopamine-dependent mechanism’, *Neuropharmacology*, vol. 52, no. 4, pp. 1169–1178, Mar. 2007, doi: 10.1016/j.neuropharm.2006.12.005.
[39] A. Donini and A. B. Lange, ‘Evidence for a possible neurotransmitter/neuromodulator role of tyramine on the locust oviducts’, *J. Insect Physiol.*, vol. 50, no. 4, pp. 351–361, Apr. 2004, doi: 10.1016/j.jinsphys.2004.02.005.
[40] C. McClung and J. Hirsh, ‘The trace amine tyramine is essential for sensitization to cocaine in Drosophila’, *Curr. Biol.*, vol. 9, no. 16, pp. 853–860, Aug. 1999, doi: 10.1016/S0960-9822(99)80389-3.
[41] M. A. El-Brolosy and D. Y. R. Stainier, ‘Genetic compensation: A phenomenon in search of mechanisms’, *PLOS Genet.*, vol. 13, no. 7, p. e1006780, Jul. 2017, doi: 10.1371/journal.pgen.1006780.
[42] A. A. Prinz, D. Bucher, and E. Marder, ‘Similar network activity from disparate circuit parameters’, *Nat. Neurosci.*, vol. 7, no. 12, pp. 1345–1352, Dec. 2004, doi: 10.1038/nn1352.
[43] E. Marder, ‘Neuromodulation of Neuronal Circuits: Back to the Future’, *Neuron*, vol. 76, no. 1, pp. 1–11, Oct. 2012, doi: 10.1016/j.neuron.2012.09.010.
[44] E. Marder, ‘Variability, compensation, and modulation in neurons and circuits’, *Proc. Natl. Acad. Sci.*, vol. 108, no. supplement_3, pp. 15542–15548, Sep. 2011, doi: 10.1073/pnas.1010674108.
[45] M. Selcho, D. Pauls, A. Huser, R. F. Stocker, and A. S. Thum, ‘Characterization of the octopaminergic and tyraminergic neurons in the central brain of *Drosophila* larvae’, *J. Comp. Neurol.*, vol. 522, no. 15, pp. 3485–3500, Oct. 2014, doi: 10.1002/cne.23616.
[46] S. R. Pulver, T. G. Bayley, A. L. Taylor, J. Berni, M. Bate, and B. Hedwig, ‘Imaging fictive locomotor patterns in larval Drosophila.’, *J. Neurophysiol.*, vol. 114, no. 5, pp. 2564–2577, Nov. 2015, doi: 10.1152/jn.00731.2015.
[47] W. C. Lemon *et al.*, ‘Whole-central nervous system functional imaging in larval Drosophila.’, *Nat. Commun.*, vol. 6, p. 7924, Aug. 2015, doi: 10.1038/ncomms8924.
[48] A. Sordillo and C. I. Bargmann, ‘Behavioral control by depolarized and hyperpolarized states of an integrating neuron’, *eLife*, vol. 10, p. e67723, Nov. 2021, doi: 10.7554/eLife.67723.
[49] J. K. Pirri, A. D. McPherson, J. L. Donnelly, M. M. Francis, and M. J. Alkema, ‘A Tyramine-Gated Chloride Channel Coordinates Distinct Motor Programs of a Caenorhabditis elegans Escape Response’, *Neuron*, vol. 62, no. 4, pp. 526–538, May 2009, doi: 10.1016/j.neuron.2009.04.013.
[50] Y. Kagawa-Nagamura, K. Gengyo-Ando, M. Ohkura, and J. Nakai, ‘Role of tyramine in calcium dynamics of GABAergic neurons and escape behavior in Caenorhabditis elegans’, *Zool. Lett.*, vol. 4, no. 1, p. 19, Dec. 2018, doi: 10.1186/s40851-018-0103-1.
[51] J. Meng *et al.*, ‘A tonically active master neuron modulates mutually exclusive motor states at two timescales’, *Sci. Adv.*, vol. 10, no. 15, p. eadk0002, Apr. 2024, doi: 10.1126/sciadv.adk0002.
[52] R. Marley and R. A. Baines, ‘Dissection of Third-Instar *Drosophila* Larvae for Electrophysiological Recording from Neurons’, *Cold Spring Harb. Protoc.*, vol. 2011, no. 9, p. pdb.prot065656, Sep. 2011, doi: 10.1101/pdb.prot065656.

[53] S. H. Cole, G. E. Carney, C. A. McClung, S. S. Willard, B. J. Taylor, and J. Hirsh, 'Two Functional but Noncomplementing Drosophila Tyrosine Decarboxylase Genes', *J. Biol. Chem.*, vol. 280, no. 15, pp. 14948–14955, Apr. 2005, doi: 10.1074/jbc.M414197200.

[54] A. Edelstein, N. Amodaj, K. Hoover, R. Vale, and N. Stuurman, 'Computer Control of Microscopes Using μManager', *Curr. Protoc. Mol. Biol.*, vol. 92, no. 1, Oct. 2010, doi: 10.1002/0471142727.mb1420s92.

[55] C. A. Schneider, W. S. Rasband, and K. W. Eliceiri, 'NIH Image to ImageJ: 25 years of image analysis', *Nat. Methods*, vol. 9, no. 7, pp. 671–675, Jul. 2012, doi: 10.1038/nmeth.2089.

[56] J. Schindelin *et al.*, 'Fiji: an open-source platform for biological-image analysis', *Nat. Methods*, vol. 9, no. 7, pp. 676–682, Jul. 2012, doi: 10.1038/nmeth.2019.

[57] W. J. Heitler, 'Practical tools for analysing rhythmic neural activity', *J. Neurosci. Methods*, vol. 185, no. 1, pp. 151–164, Dec. 2009, doi: 10.1016/j.jneumeth.2009.09.009.

[58] J. Berni, 'Genetic dissection of a regionally differentiated network for exploratory behavior in Drosophila larvae.', *Curr. Biol. CB*, vol. 25, no. 10, pp. 1319–1326, May 2015, doi: 10.1016/j.cub.2015.03.023.

[59] M. Monastirioti, C. E. Linn, Jr., and K. White, 'Characterization of ***Drosophila Tyramine β-Hydroxylase*** Gene and Isolation of Mutant Flies Lacking Octopamine', *J. Neurosci.*, vol. 16, no. 12, pp. 3900–3911, Jun. 1996, doi: 10.1523/JNEUROSCI.16-12-03900.1996.

[60] A. Debnath, P. D. E. Williams, and B. A. Bamber, 'Reduced Ca2+ transient amplitudes may signify increased or decreased depolarization depending on the neuromodulatory signaling pathway', *Front. Neurosci.*, vol. 16, p. 931328, Jul. 2022, doi: 10.3389/fnins.2022.931328.

[61] M. Winding *et al.*, 'The connectome of an insect brain', *Science*, vol. 379, no. 6636, p. eadd9330, Mar. 2023, doi: 10.1126/science.add9330.

[62] T. Stürner *et al.*, 'Comparative connectomics of the descending and ascending neurons of the *Drosophila* nervous system: stereotypy and sexual dimorphism', Jun. 06, 2024. doi: 10.1101/2024.06.04.596633.

[63] A. A. Zarin, B. Mark, A. Cardona, A. Litwin-Kumar, and C. Q. Doe, 'A multilayer circuit architecture for the generation of distinct locomotor behaviors in *Drosophila*', *eLife*, vol. 8, p. e51781, Dec. 2019, doi: 10.7554/eLife.51781.

[64] A. Fushiki, M. F. Zwart, H. Kohsaka, R. D. Fetter, A. Cardona, and A. Nose, 'A circuit mechanism for the propagation of waves of muscle contraction in Drosophila', *eLife*, vol. 5, p. e13253, Feb. 2016, doi: 10.7554/eLife.13253.

[65] A. Carreira-Rosario *et al.*, 'MDN brain descending neurons coordinately activate backward and inhibit forward locomotion', *eLife*, vol. 7, p. e38554, Aug. 2018, doi: 10.7554/eLife.38554.

[66] A. Zhao *et al.*, 'High-ambition climate action in all sectors can achieve a 65% greenhouse gas emissions reduction in the United States by 2035', *Npj Clim. Action*, vol. 3, no. 1, p. 63, Jul. 2024, doi: 10.1038/s44168-024-00145-x.

[67] U. Černe *et al.*, 'Ca^{2+} excitability of glia to neuromodulator octopamine in *Drosophila* living brain is greater than that of neurons', *Acta Physiol.*, vol. 241, no. 2, p. e14270, Feb. 2025, doi: 10.1111/apha.14270.

[68] S. El-Kholy, F. Stephano, Y. Li, A. Bhandari, C. Fink, and T. Roeder, 'Expression analysis of octopamine and tyramine receptors in Drosophila', *Cell Tissue Res.*, vol. 361, no. 3, pp. 669–684, Sep. 2015, doi: 10.1007/s00441-015-2137-4.

[69] L. M. Sherer *et al.*, 'Octopamine neuron dependent aggression requires dVGLUT from dual-transmitting neurons', *PLOS Genet.*, vol. 16, no. 2, p. e1008609, Feb. 2020, doi: 10.1371/journal.pgen.1008609.

[70] C.-L. Wu, M.-F. M. Shih, P.-T. Lee, and A.-S. Chiang, 'An Octopamine-Mushroom Body Circuit Modulates the Formation of Anesthesia-Resistant Memory in Drosophila', *Curr. Biol.*, vol. 23, no. 23, pp. 2346–2354, Dec. 2013, doi: 10.1016/j.cub.2013.09.056.

[71] J. Li and W. L. Shew, ‘Tuning network dynamics from criticality to an asynchronous state’, *PLOS Comput. Biol.*, vol. 16, no. 9, p. e1008268, Sep. 2020, doi: 10.1371/journal.pcbi.1008268.